European Journal of Medicinal Chemistry 293 (2025) 117736

Contents lists available at ScienceDirect

European Journal of Medicinal Chemistry

journal homepage: www.elsevier.com/locate/ejmech

Research paper

Design, synthesis and characterization of aryl bis-guanyl hydrazones as RNA binders of *C9orf72* G_4C_2 extended repeats

Alice Maiocchi [a,1,3], Martina Pedrini [a,3,2], Veronica Ferrari [b,3], Agata Sofia Assunçao Carreira [c,3], Vincenzo Maria D'Amore [d,3], Federica Santoro [d], Anna Di Porzio [d], Maddalena Bosetti [c], Riccardo Cristofani [b], Alessandra Silvani [a], Diego Brancaccio [d], Luciana Marinelli [d], Francesco Saverio Di Leva [d,*], Alessandro Provenzani [c,**], Angelo Poletti [b,***], Pierfausto Seneci [a,****]

[a] Chemistry Department, Università degli Studi di Milano, Via Golgi 19, 20133, Milan, Italy
[b] Dipartimento di Scienze Farmacologiche e Biomolecolari (DisFeB) "Rodolfo Paoletti", Università degli Studi di Milano, Via Balzaretti 9, 20133, Milan, Italy
[c] Laboratory of Genomic Screening, Department of Cellular, Computational and Integrative Biology, University of Trento, Via Sommarive 9, Povo, 38123, (TN), Italy
[d] Department of Pharmacy, Università degli Studi di Napoli Federico II, via D. Montesano 49, 80131, Napoli, Italy

ARTICLE INFO

Keywords:
Guanyl hydrazones
Expanded G_4C_2 repeats
C9orf72 gene
RNA transcripts
NMR binding studies
RNA-Small molecule modeling
ALS

ABSTRACT

Expanded G_4C_2 repeats derived from mutations of the *C9orf72* gene are causative factors in amyotrophic lateral sclerosis (ALS) and frontotemporal dementia (FTD) patients, leading to multiple pathological events. Bis thiophene *para* dinicotinimidamide **2a** was reported to preferentially stabilize G-quadruplex G_4C_2 RNA structures at sub-micromolar concentrations. We replaced its amidine groups with BBB-compliant guanyl hydrazones, and carried out scaffold variations to improve water solubility. An eight-membered array was built around bis-thiophene- (**4b-6a**), bis-oxazole- (**7b**), diphenylurea diamide- (**8b**) and phenyldioxy ditriazolephenyl scaffolds (**9a,b**). Biological profiling of the array identified **4b** as a promising, drug-like hit, active in cellular assays on ALS patient-derived cells.

1. Introduction

The therapeutic relevance and number of RNA-interfering candidates are steadily growing in the last decades [1]. Biological efforts centered on antisense oligonucleotides (ASOs) and short interfering RNAs (siRNAs) were recently complemented by clustered regularly interspaced short palindromic repeats/CRISPR-associated protein 9 (CRISPR-CAS9) approaches [2]. Although some entered clinical trials, they are still hampered by limited delivery options [3], and by the risk of off-target toxicity and immunogenicity [1].

A complementary, possibly safer approach to RNA targeting is represented by low-molecular weight organic compounds. Small molecule RNA-binding drugs have been known since aminoglycoside antibiotics, that interfere with prokaryotic ribosomal RNA [4]. Recently, risdiplam was approved as a treatment for spinal muscular atrophy, acting as a splicing enhancer for the survival motor neuron 2 (SMN2) protein through stabilization of an adenosine bulge in the exon 7 of its pre-mRNA [5]; the rapidly growing universe of RNA-binding small molecule hits and leads was recently reviewed [6,7]. The identification and structural optimization of small molecule RNA binders benefit from available assay formats for RNA-targeted high throughput screening [8], from the availability of numerous RNA structures [9] and of

* Corresponding author.
** Corresponding author.
*** Corresponding author.
**** Corresponding author.
E-mail addresses: francesco.dileva@unina.it (F.S. Di Leva), alessandro.provenzani@unitn.it (A. Provenzani), angelo.poletti@unimi.it (A. Poletti), pierfausto.seneci@unimi.it (P. Seneci).
[1] Present address: Olon SpA, Via B. Cellini 20, 20090 Segrate (MI), Italy.
[2] Present address: Procos SpA, Via G. Matteotti 249, 28062 Cameri (NO), Italy.
[3] The authors wish it to be known that, in their opinion, these authors should be regarded as joint First Authors.

https://doi.org/10.1016/j.ejmech.2025.117736
Received 30 January 2025; Received in revised form 28 April 2025; Accepted 6 May 2025
Available online 7 May 2025

RNA-targeted collections of drug-like small molecules [10,11].

Amyotrophic lateral sclerosis (ALS) [12] is a heterogeneous, late-onset, fatal neurodegenerative disease characterized by progressive loss of the upper and lower motor neurons at the spinal or bulbar level; both a most common sporadic ALS (sALS, ≈90 % of total cases) and familial-type ALS (fALS, ≈10 %), characterized by an associated genetic dominant inheritance factor, are observed [13]. Frontotemporal dementia (FTD) entails the progressive degeneration of frontal and temporal brain lobes leading to diverse types of dementia [14]; a significant proportion of FTD patients shows a familial component related to a variety of genes [15].

A short G_4C_2 hexanucleotide repeat (≤11 repeats) is present in the first intron of the highly conserved *C9orf72* gene; its pathological expansion, up to several thousand repeats, is found in ALS and FTD patients [16]. Expanded G_4C_2 DNA/RNA repeats and epigenetic mechanisms reduce the physiological transcription process of the downstream gene, causing a loss-of-function phenotype. RNA repeats disturb the nucleo-cytoplasmatic transport by altering the Nuclear Pore Complex (NPC) functionality [17], and form neurotoxic RNA foci aggregates, disturbing RNA metabolism [18]. Moreover, they promote noncanonical repeat-associated non-AUG-dependent (RAN) translation of expanded RNA to five dipeptide protein repeats (DPRs) from sense G_4C_2 RNA (poly (GR) and poly(GA)), antisense C_4G_2 RNA (poly(PR) and poly(PA)) and both (poly(GP)), that cause nuclear and cytoplasmic cellular toxicity [19].

C9orf72-targeted ASOs entered clinical trials, but their development was recently halted due to limited efficacy and toxicity issues [20]; other biologicals are under preclinical development [21]. Small molecule hits were reported as targeting either the hairpin or the G-quadruplex conformations which can be alternatively formed by G_4C_2 repeats [22,23]; the latter conformations are targeted also by the marine natural product chrexanthomycins [23] and by pyridostatin [24]. In particular, symmetrical bis heteroaryl *para* dinicotinimidamides **1a-3a** (Fig. 1) showed preferential stabilization of the G-quadruplex structure of G_4C_2 RNAs at sub-micromolar concentrations [25]; we reasoned that their amidine groups could be replaced by more BBB-compliant substituents, earlier

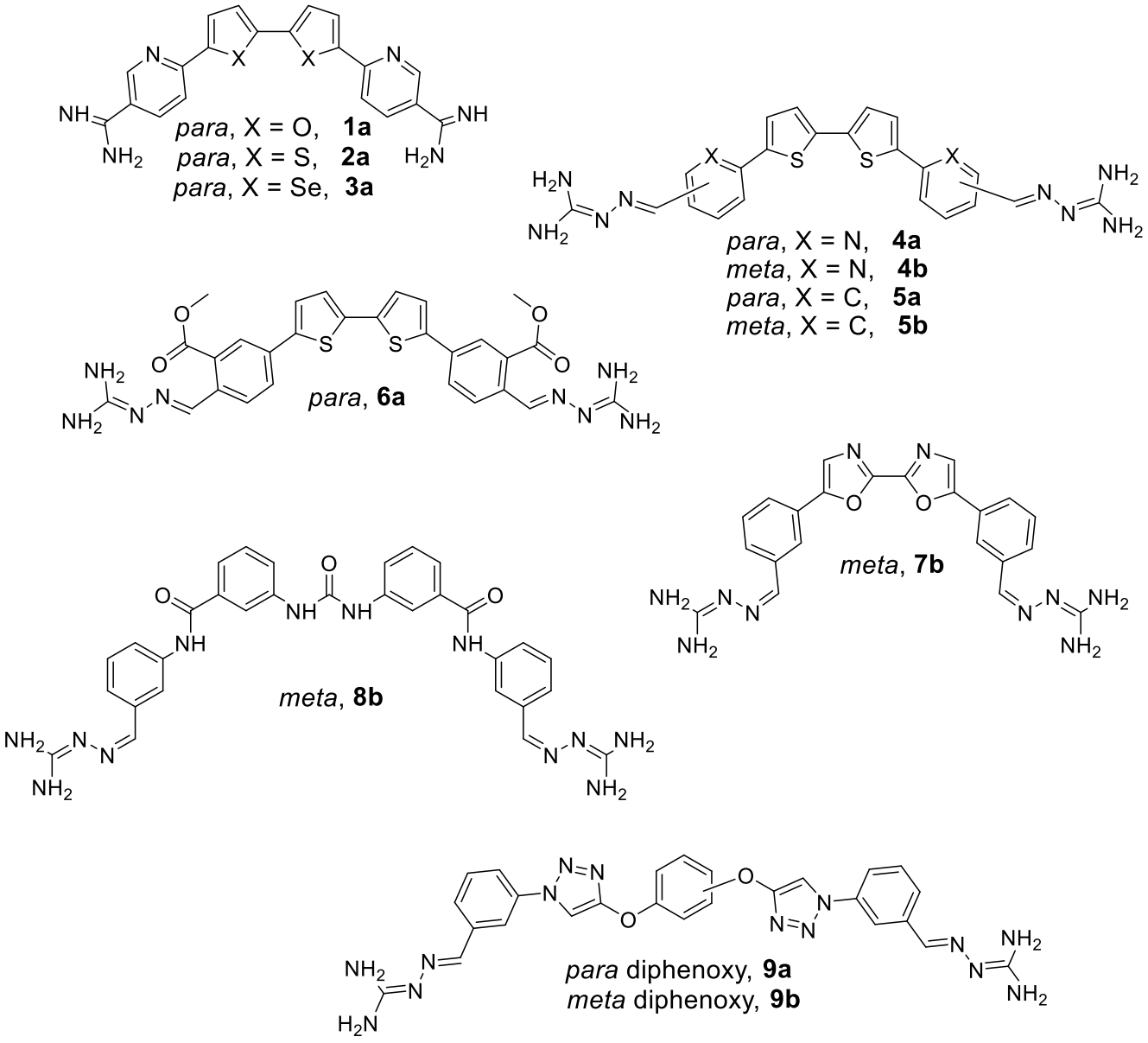

Fig. 1. Structure of bis heteroaryl *para* dinicotinimidamides **1a-3a**, bis-thiophene(hetero)aryl *para*- and *meta* diguanyl hydrazones **4a-6a**, bis-oxazolephenyl *meta* diguanyl hydrazone **7b**, *meta* diphenylurea diamide *meta* diguanyl hydrazone **8b**, and *para* and *meta* phenyldioxy ditriazolearyl *meta* guanyl hydrazones **9a,b**.

reported by some of us as leads for CNS indications [26,27].

In particular, we focused on bis-thiophene **2a** and replaced its amidines with guanyl hydrazones, to lower its pK_a and ensure higher BBB penetration [28]. Considering their larger volume with respect to amidines, guanyl hydrazones were strategically placed in *para*- and *meta*, (**4a** and **4b**, Fig. 1). We also replaced the pyridines with phenyl rings, as in *para*- **5a** and *meta*-substituted **5b**; and we introduced a third substituent on the phenyl rings, as in *para* substituted **6a** (Fig. 1). Finally, in a scaffold hopping approach we replaced the core bis thiophene ring with a conservative (*meta* bis-oxazole, **7b**) and three diverse scaffolds (diphenylurea *meta* substituted diamide **8b**, 1,4- and 1,3 diphenol *meta* substituted phenyltriazoles **9a** and **9b**, Fig. 1).

The array of eight putative expanded RNA G_4C_2 repeat binders was biologically profiled on multiple cell lines, with various readouts to determine their potential as *C9orf72* RNA binders. The bis-thiophenepyridyl *meta* diguanyl hydrazone **4b** turned out to be most active, well tolerated in neuronal cells and selective in decreasing sense DPRs poly(GA) and poly(GP) repeats.

2. Results

2.1. Synthesis

Guanyl hydrazones (GHs from now on) show pK_a ranges close to neutrality, due to electronic delocalization (Fig. 2: azine form – favoured, representing GHs in each Figure and Scheme, vs. hydrazone form – disfavoured; ≥15 % neutral species at physiological pH [28,29]). Therefore, GHs should be able to exploit ionic interactions with negatively charged $(G_4C_2)_n$ repeats; their presence in BBB-permeable drugs [30], *in vivo* active leads against peripheral (PNS) [26] and central nervous system (CNS) diseases [27] supports their bioavailability.

*Bis-thiophene(hetero)aryl para and meta di-GHs **4a-6b***. Our synthetic strategy entailed the assembly of the bis-thiophenearyl tetracyclic system through a Suzuki coupling between bis-thiophene diboron pinacolate ester and, respectively, 6-bromopyridine 3- (**I**) and 2-carboxaldehyde (**II**); 4-bromo (**III**) and 3-bromobenzaldehyde (**IV**); and methyl 5-bromo 2-formylbenzoate (**V**) (step a, Scheme 1).

Most Suzuki couplings in standard conditions led to good to excellent yields, but only traces of target dialdehyde **11a** were observed with 6-bromopyridine 3-carboxaldehyde **I**, even varying reaction time and temperature, base and solvent; thus, the synthesis of target **4a** was abandoned.

Bis-thiophenearyl dialdehydes **11b-13a** were condensed in catalytic acid conditions with sub-stoichiometric amounts of aminoguanidine hydrochloride (AG.HCl from now on), to avoid the removal of excess AG.HCl (step b, Scheme 1). Pure target (hetero))aryl di-GHs **4b-6a** were obtained in good to excellent yields after simple work-ups and, when needed, reverse phase chromatographic purifications.

Reagents and conditions: (a) **I** to **V**, $Pd(PPh_3)_4$, K_2CO_3, N_2, dry DMF, 80 °C, 12 h, **11a** (traces), **11b** (78 %), **12a** (84 %), **12b** (52 %), **13a** (63 %); b) AG.HCl, cat. HCl, EtOH, reflux, 8 h, **4b** (92 %), **5a** (72 %), **5b** (65 %), **6a** (94 %).

*Bis-oxazolephenyl meta di-GH **7b***. Bis-oxazole-centered *meta* analogue **7b** was obtained through a five steps' synthesis from protected 3-bromobenzaldehyde (Scheme 2), adapting a reported route [31].

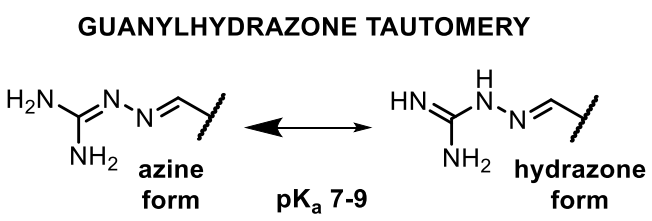

Fig. 2. Tautomery and pK_a range of GHs.

Formylation with DMF (step a) followed by condensation with toluenesulfonylmethyl isocyanide (TosMIC) led to protected oxazole *meta* aldehyde **15b** in good yields (step b). Then, a palladium/copper-induced oxidative coupling (step c) yielded protected tetraaryl intermediate **16b** in good yields; after aldehyde deprotection in acidic conditions (step d) and standard AG.HCl coupling (step e, Scheme 2) pure target bis-oxazolephenyl *meta* di-GH **7b** was obtained in overall moderate yields.

Reagents and conditions: (a) n-BuLi, dry THF, N_2, -78 °C, 40 min, then dry DMF, −78 °C, 2 h, 53 %; (b) K_2CO_3, TosMIC, dry MeOH, N_2, 65 °C, 5 h, 88 %; (c) $PdCl_2$, PPh_3, CuCl, $Cu(OAc)_2$, 10:1 dry 1,4-dioxane/dry DMSO, N_2, 120 °C, 4 h, 66 %; (d) 1 M aq. HCl, 80 °C, 5 h, 74 %; (e) AG.HCl, cat. HCl, EtOH, 80 °C, 12 h, 60 %.

*Meta diphenylurea meta aryl di-GH **8b***. Diphenylurea-centered analogue **8b** was obtained through a five steps' synthesis from C-protected 3-aminobenzoic acid (Scheme 3). Its reaction with carbonyl diimidazole (CDI, step a) and pivaloyl ester deprotection in acidic conditions (step b) yielded urea *meta*-dicarboxylic acid intermediate **19** in excellent yields. Its amidation with C-protected 3-aminobenzaldehyde (step c) and acidic deprotection (step d) led to good yields of *meta* dialdehyde **21b**, then submitted to standard AG.HCl condensation (step e, Scheme 3) to pure target *meta* diphenylurea *meta* aryl-di-GH **8b** in overall good yields.

Reagents and conditions: (a) CDI, dry THF, N_2, 60 °C, 5 h, 82 %; (b) TFA, r.t., 16 h, quantitative; (c) HATU, DIPEA, HOBt, dry DMF, N_2, r.t., 16 h, 74 %; (d) 1:1 1 M aq. HCl/1,4-dioxane, 55 °C, 16 h, 86 %; (e) AG.HCl, cat. HCl, EtOH, 80 °C, 12 h, 96 %.

*Para- and meta-phenyldioxy ditriazolearyl meta di-GHs **9a,b***. Ditriazolyloxyphenyl-centered analogs **9a,b** were obtained through a six steps' synthesis from *para/meta* diphenols and ethyl 3-aminobenzoate (Scheme 4).

Commercial reagents were converted to ethyl 3-azidobenzoate **22** (step a, diazotation – azidation of ethyl 3-aminobenzoate), to *para*- and *meta*-dipropargyl ethers **23a,b** (step b, alkylation of diphenols with propargyl bromide). A click reaction in standard conditions (step c) yielded diphenylurea-centered diesters **24a,b** in good yields. A reduction – partial oxidation cycle (step d – **25a,b**, step e – Dess Martin periodinane (DMP)) afforded dialdehydes **26a,b**, converted to pure *para*-, *meta*-phenyldioxy ditriazolearyl di-GHs **9a,b** by standard AG.HCl condensation in overall good yields (step f, Scheme 4).

Reagents and conditions: (a) H_2SO_4, $NaNO_2$, H_2O, 0 °C, 15 min, then NaN_3, r.t., 2 h, 86 %; (b) diphenol, propargyl bromide, K_2CO_3, dry acetonitrile, 70 °C, 7 h, then 16 h, r.t., **23a** (89 %), **23b** (93 %); (c) $CuSO_4.5H_2O$, sodium ascorbate, 1:1 tBuOH/H_2O, r.t., 24 h, **24a** (46 %), **24b** (68 %); (d) 1 M DIBAL-H in THF, dry THF, N_2, -70 °C, 2 h, then r.t., 16 h, **25a** (56 %), **25b** (82 %); (e) DMP, dry CH_2Cl_2, r.t., 24 h, **26a** (90 %), **26b** (97 %); (f) AG.HCl, cat. 1 N HCl, EtOH, 80 °C, 8 h, **9a** (72 %), **9b** (97 %).

Thus, a small array of eight putative RNA binders - bis-thiophene (hetero)aryl *meta*- and *para* di-GHs **4b-6b**, bis-oxazolephenyl *meta* di-GH **7b**, *meta* diphenylurea *meta* di-GH **8b**, *para*- and *meta*phenyldioxy ditriazolearyl *meta* di-GHs **9a,b** – was sent to biological profiling.

2.2. Primary screening of (hetero)aryl di-GHs 4b–9b

Prior to testing our compounds' ability to decrease DPRs produced from $(G_4C_2)_n$ expansions, we determined their cytotoxicity and identified a molecule-specific concentration for safe activity testing (test concentration). HEK293T cells were treated for 24 h with increasing concentrations (0.3125–40 μM) of (hetero)aryl di-GHs **4b**–**9b**. Cell viability was assessed through a metabolic assay (Fig. 3A), which determined a 50 % cytotoxicity concentration (CC_{50}) value for each putative RNA binder with the exception of **8b** (Fig. 3A).

Selected test concentrations for subsequent activity testing were slightly lower than their CC_{50}, with the exception of **7b**, to minimize the risk of cellular toxicity (Fig. 3, Panel A). To further confirm that hetero) aryl di-GHs **4b**–**9b** were well tolerated by HEK293T cells, we performed

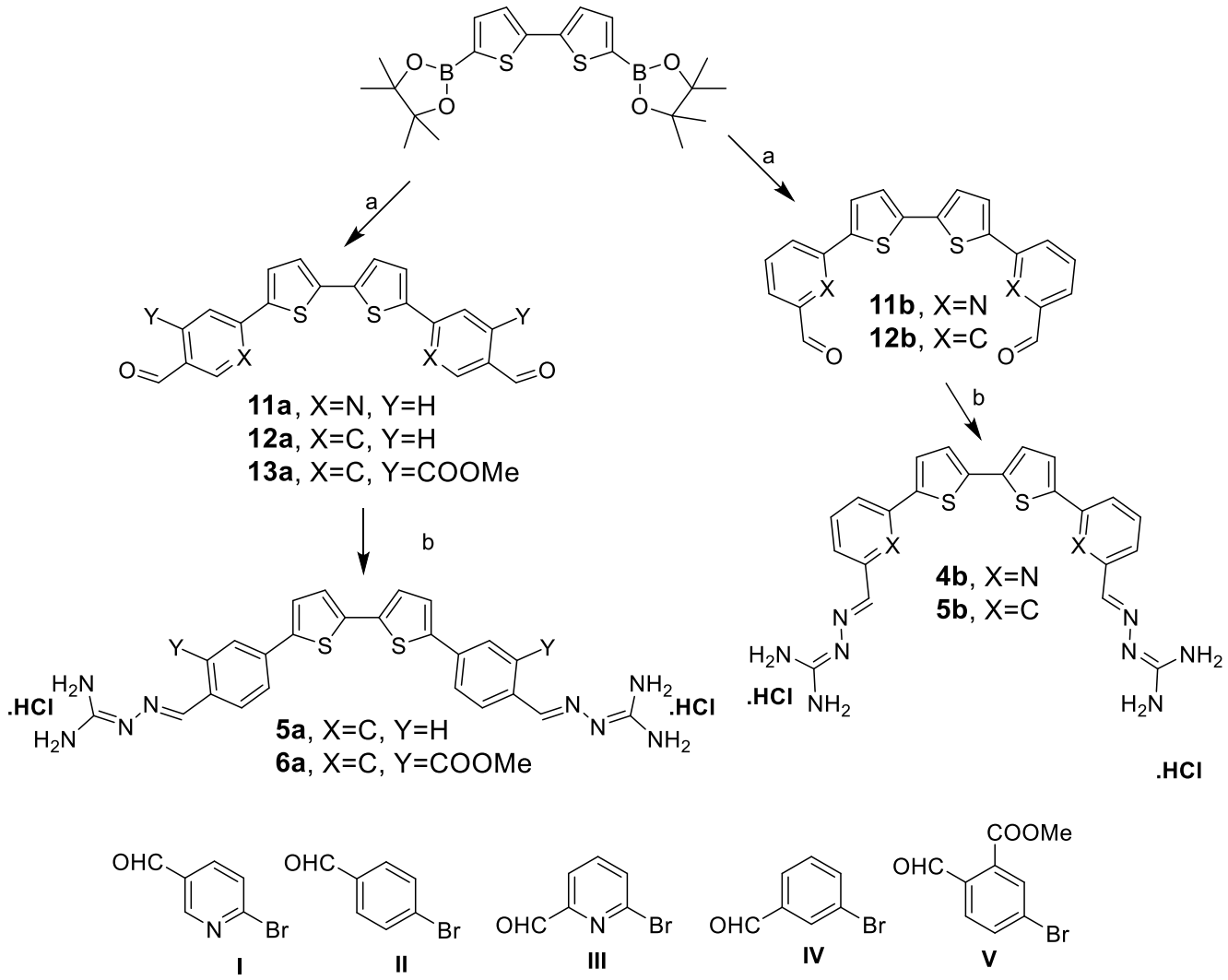

Scheme 1. Synthesis of bis-thiophene(hetero)aryl *para* and *meta* di-GHs **4a-6a**.

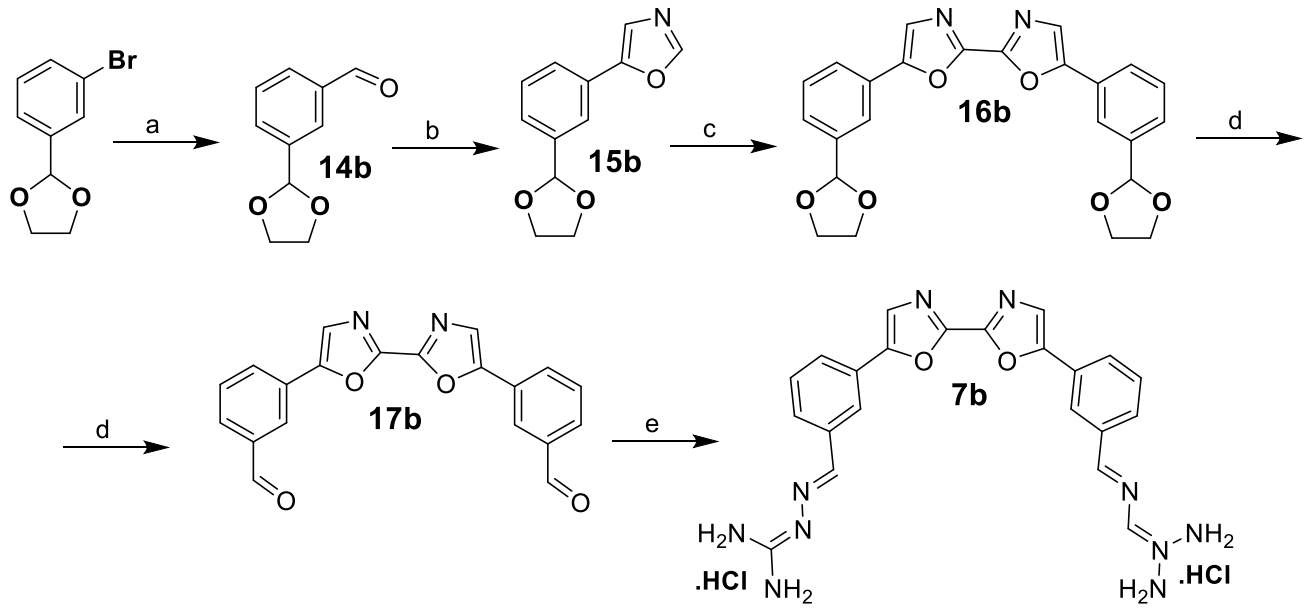

Scheme 2. Synthesis of bis-oxazolephenyl *meta* di-GH **7b**.

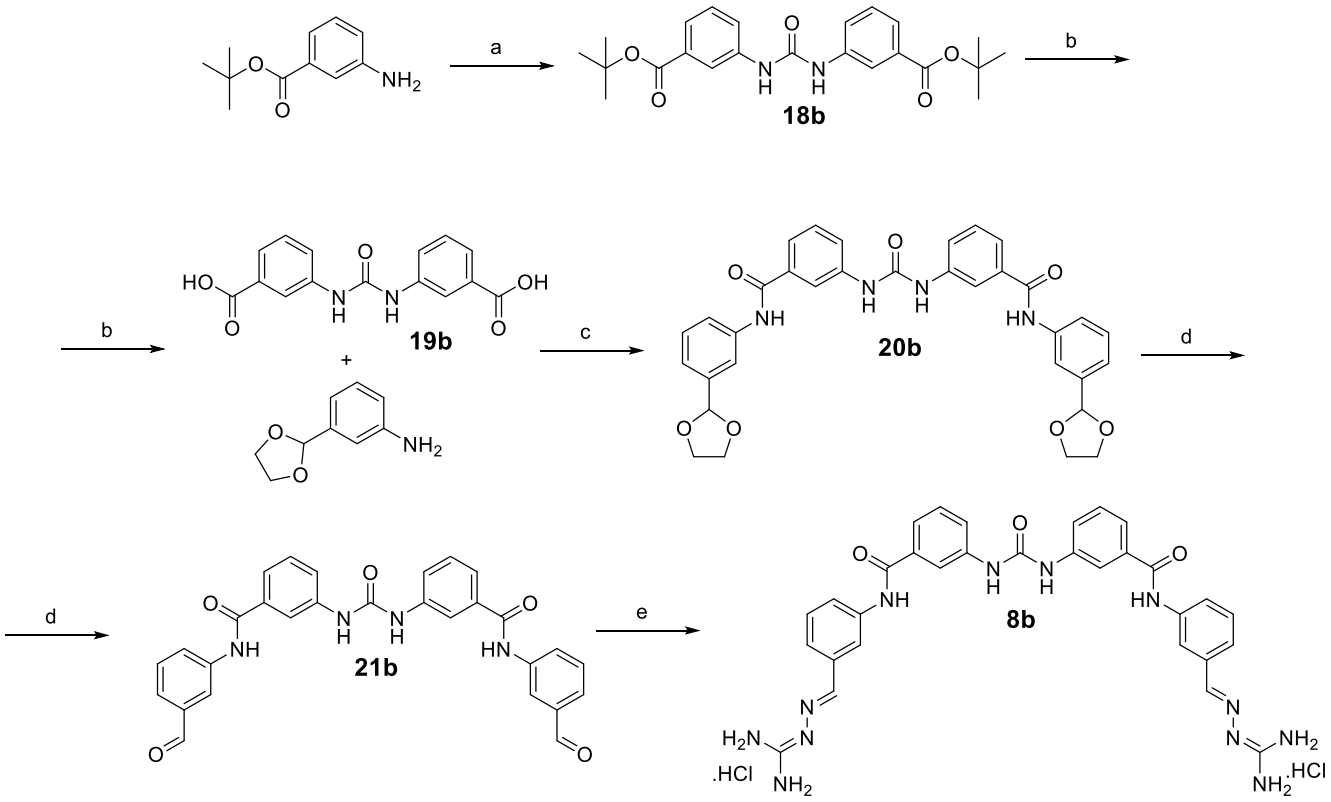

Scheme 3. Synthesis of *meta* diphenylurea *meta* di-GH **8b**.

the lactate dehydrogenase (LDH) assay (Fig. 3, Panel B). As plasma membrane damage releases LDH into the cell media, this assay can be used as a proxy for compounds' cytotoxicity. Cells were treated for 24 h with the appropriate testing concentration, and staurosporine was used as an apoptosis-inducing control [32]. Compounds **4b**–**9b** were well tolerated by cells at test concentrations, at variance with staurosporine which increased LDH release, as expected (Fig. 3, Panel B). Thus, we identified cell-tolerable, non-toxic concentrations for each hetero)aryl di-GH, then used to characterize compounds' activity against DPRs formation.

Primary screening was carried out in HEK293T cells transfected with a construct containing sixty-six G_4C_2 repeats (66R), flanked at 5' by 113 nucleotides containing the near-cognate CUG codon. Nucleotide sequences encoding for three different tags were placed downstream the expansion in each of the three reading frames, to optimize detection [33]. For screening purposes we assessed the high expression of poly (GA) (HA tag), since it is the most abundant translated DPR (panel A, second bar, Fig. 4A). Transfected cells were treated for 24 h with earlier selected test concentrations (Fig. 3A) for each aryl di-GH, and poly(GA) levels were detected by flow cytometry using an Alexa Fluor 488-tagged Anti-HA antibody. HEK293T cells transfected with a construct containing two 2R G_4C_2 repeats were used as negative controls, showing significantly lower poly-GA levels (panel A, first bar).

Among tested compounds, **4b** and **5b** significantly decreased poly (GA) levels (Fig. 4A; Supplementary Fig. S1, Panel A). Other array members were inactive. Please note that **4b**, likely due to its yellow color, interfered with the fluorophore signal so that its effect could not be quantified; thus, we set a **4b**-specific background condition with cells untreated with the antibody to define a negative cell population (Supplementary Fig. S1, Panel B). Compound **5a** also showed interference (Supplementary Fig. S1, Panel C), which could not be corrected with the same strategy. Consequently, to confirm the activity of **4b** and **5b** and to determine aryl di-GH **5a** efficacy in decreasing poly(GA) levels, we performed immunoblotting (Fig. 4B). All three compounds decreased poly(GA) levels, with a qualitative **4b** > **5a** ≈ **5b** ranking. Thus, we selected bis-thiophenephenyl *meta* di-GH **4b**, bis-thiophenepyridyl *para* di-GH **5a** and bis-thiophenepyridyl *meta* di-GH **5b** as initial hits for further validation in more complex cellular models.

2.3. Further profiling of heteroaryl di-GHs 4b, 5a and 5b

Initial hits **4b**, **5a** and **5b** were tested at compound-specific concentrations on small molecule neural progenitor cells (smNPCs) derived from CS52iALS-C9n6 induced pluripotent stem cells (iPSCs) for their effectiveness in reducing poly(GA) levels, and for non-specific toxic effects on smNPCs. CS52iALS-C9n6 iPSCs were reprogrammed from the fibroblasts of a C9orf72 patient. The results of such experiments are shown in Fig. 5.

A concentration-dependent decrease in the levels of poly(GA) up to 50 μM was triggered by **4b** (panel A, Fig. 5), while **5b** did not significantly affect poly(GA) levels up to 30 μM (panel C), and **5a** lacked a clear concentration-response pattern (panel B). We determined the tolerance of smNPCs for (hetero)aryl di-GHs **4b**, **5a** and **5b** through an LDH assay (panels D–F) and a 3-(4,5-dimethylthiazol-2-yl)-2,5-diphenyltetrazolium bromide (MTT) assay (panels G–I). As to the former, smNPCs were treated for 24 h with the selected testing concentration, then for 1 h with a lysis buffer as a positive control, following manufacturer's instructions. Compounds **4b** and **5a** were well tolerated by cells at test concentrations (panels D and E, Fig. 5), while **5b** showed limited, toxicity-dependent LDH release at the highest 30 μM concentration (panel F, Fig. 5). We then confirmed our results by evaluating the viability of smNPCs exposed for 24 h to selected testing concentrations of(hetero)aryl di-GHs **4b**, **5a** and **5b**, using the MTT assay (panels G–I, Fig. 5). Both **4b** and **5a** did not affect cell viability at all tested concentrations, while once more **5b** altered cell viability only at the highest 30 μM concentration. Altogether, hit compound **4b** caused a decrease in poly(GA) levels without affecting smNPC viability; **5a** and **5b** both lacked efficacy, with the latter showing minimal cell toxicity at high

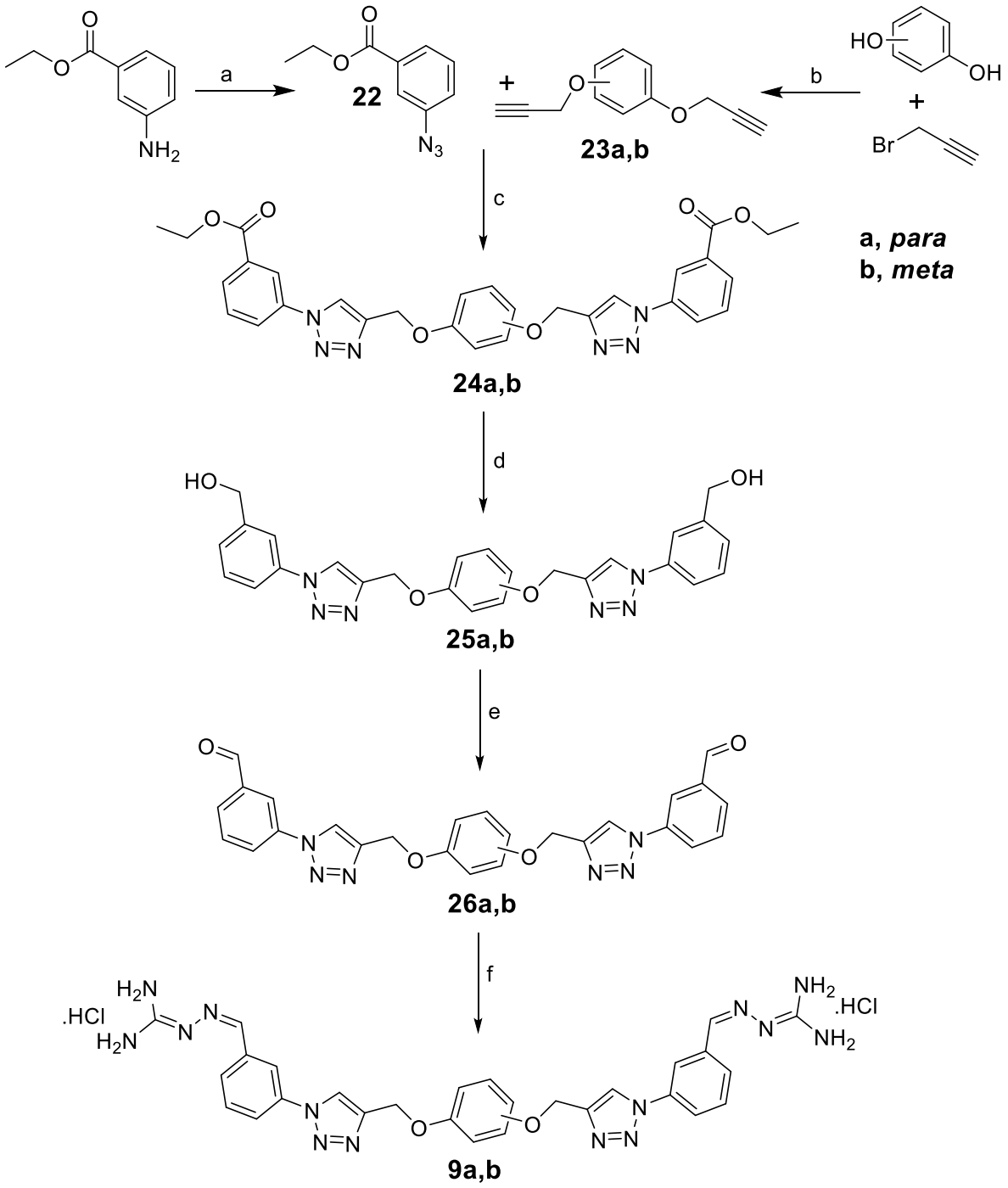

Scheme 4. Synthesis of *para* and *meta* phenyldioxy ditriazolearyl *meta* di-GHs **9a,b**.

concentrations.

We then tested the initial hits at compound-specific concentrations on motor neuron-like NSC34 cells overexpressing either 66R G_4C_2 or short 2R G_4C_2 as negative controls (Fig. 6, Panels A–C). We analyzed poly(GP) aggregate levels through the filter trap assay (FTA) which quantifies cellular levels of high molecular species; poly-GP aggregate levels are compared between NSC34 cells overexpressing short 2R G_4C_2 and extended 66R G_4C_2 repeats (respectively first and second lanes, panels A to C). Again, cytotoxic effects of (hetero)aryl di-GHs **4b**, **5a** and **5b** on NSC34 cells were determined through an LDH assay (Fig. 6, Panels D–F).

We detected a significant **4b**-induced decrease of poly(GP) levels; conversely, **5a** showed lower efficacy at lower, non-cytotoxic concentrations, while **5b** was inactive. Regarding cytotoxicity, compound **5a** was well tolerated at each tested concentration (Fig. 6, Panel E); LDH levels were not increased at any **5a** concentration. Both **4b** and **5b** showed limited, dose-dependent cytotoxicity with increased LDH release at the highest tested concentration - 50 μM for **4b**, 30 μM for **5b** (Fig. 6, Panels D, F). The increased, LDH-assessed cytotoxicity of **4b** at 50 μM may justify the increase of poly(GP) levels observed at this concentration (Fig. 6, Panel A; see also its 22 μM cytotoxicity in HEK293T cells, Fig. 3). Accordingly, **4b** was tested in the following studies up to 25 μM.

Altogether, these experiments prompted us to select heteroaryl di-

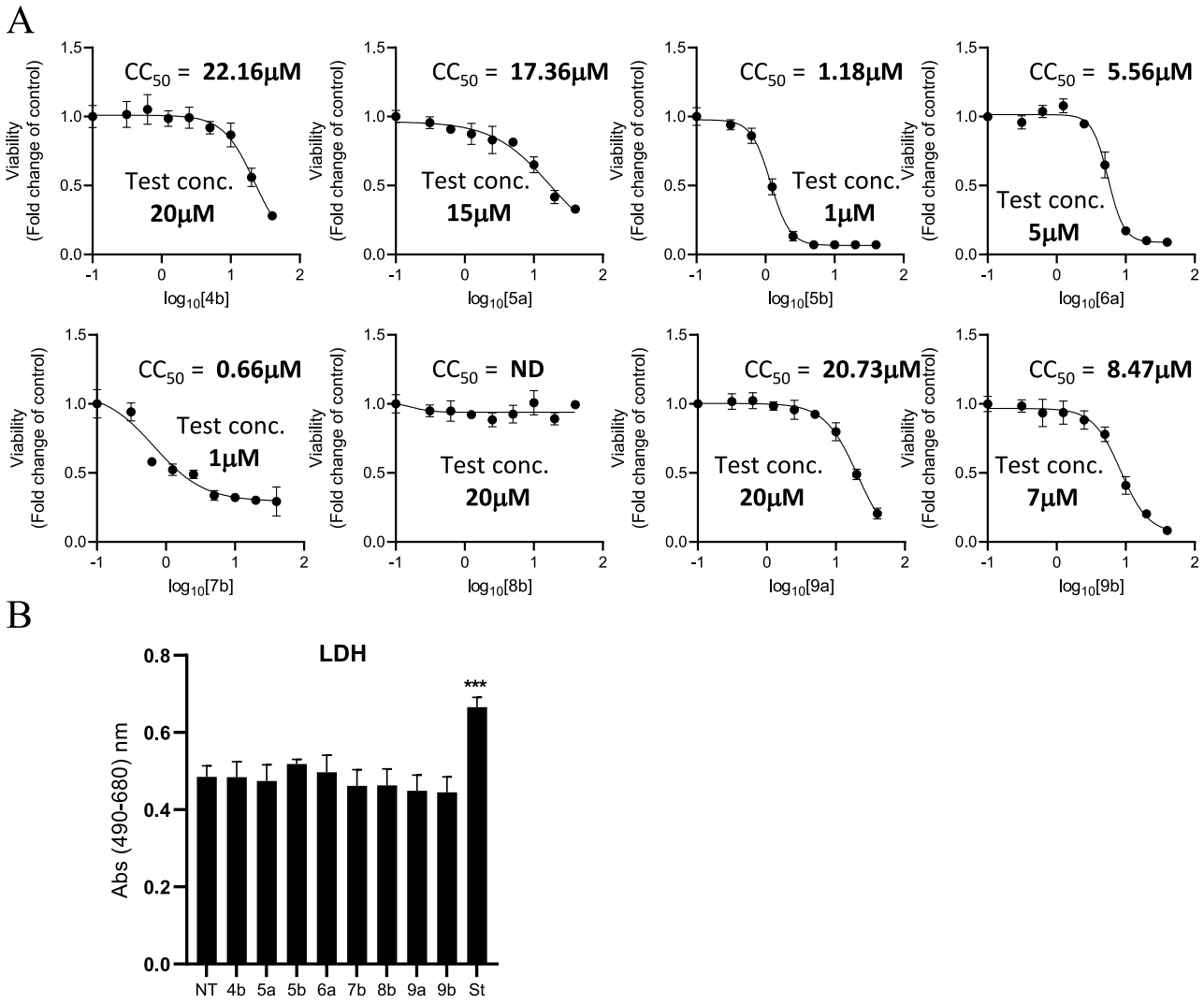

Fig. 3. Cytotoxicity of (hetero)aryl di-GHs 4b-9b in HEK293T cells. (A) CC_{50} were assessed with the OzBlue assay in HEK293T cells, after 24 h of treatment with the (hetero)aryl di-GHs **4b** (top left) - **9b** (bottom right), with concentrations-response curves ranging from 0.325 to 40 μM (8 conc.). Viability values were normalized to the control (DMSO) condition. ND, not determined. (B) LDH cytotoxicity assay performed at each compound-specific test concentration (**4b**–20 μM; **5a** – 15 μM; **5b**–1 μM: **6a** – 5 μM; **7b**–1 μM; **8b**–20 μM; **9a** – 20 μM; **9b**–7 μM) after 24 h of treatment of HEK293T cells with **4b**–**9b**. The apoptosis inducer staurosporine was used as a positive control. LDH release values were normalized to the control (DMSO) control condition. The Welch's test was used to calculate statistical significance (ns-non-significant, ***$p < 0.001$) between control- and **4b**–**9b** – tested cells.

GH **4b**, endowed with both moderate activity against poly(GA) and poly (GP) levels, for further biological and biophysical (nuclear magnetic resonance, NMR) profiling as a representative of aryl di-GHs as G_4C_2 repeat binders.

2.4. Specificity and selectivity profiling - heteroaryl di-GH 4b

As the next step in our profiling cascade, we determined the activity of **4b** on NSC34 cells transfected with three plasmids carrying a modified sequence of *C9orf72* expansion to encode respectively for poly(GA), poly (GP) and poly(PR) Fig. 7, Panels A–C; first lanes, non transfected control cells).

Heteroaryl di-GH **4b** significantly decreased sense DPRs poly(GA) and poly(GP), while being ineffective on antisense DPR poly(PR) (Fig. 7, Panels A–C). These results may suggest a sense selectivity for **4b**; the absence of CAG repeats in the plasmids with modified *C9orf72* expansion sequences indicates that **4b** elicits additional molecular interactions, to be elucidated in the near future.

To assess its selectivity against *C9orf72*-unrelated transcripts, we tested **4b** on NSC34 cells transfected with a pCMV-β-galactosidase plasmid through a β-galactosidase assay, which quantifies the enzyme expression levels by measuring its activity on its ortho-nitrophenyl-β-galactoside (ONPG) substrate, in presence of **4b** (Fig. 8).

β-Galactosidase activity and levels were not affected by **4b** at any tested concentration, suggesting a lack of interaction between **4b** and β-galactosidase mRNA, which does not contain repetitions, and supporting its selective affinity for G_4C_2 expansions.

2.5. NMR and molecular modeling studies - heteroaryl di-GH 4b

We aimed to confirm a molecular interaction between **4b** and the G_4C_2 RNA sequence by using 1D ^{1}H NMR spectroscopy. Experiments were performed under conditions favoring either a quadruplex (G4, potassium ion-containing buffer) [34] or a hairpin (sodium ion-containing buffer) [22] RNA folding. Under G4-forming conditions, the addition of **4b** led to marked chemical shift perturbations and

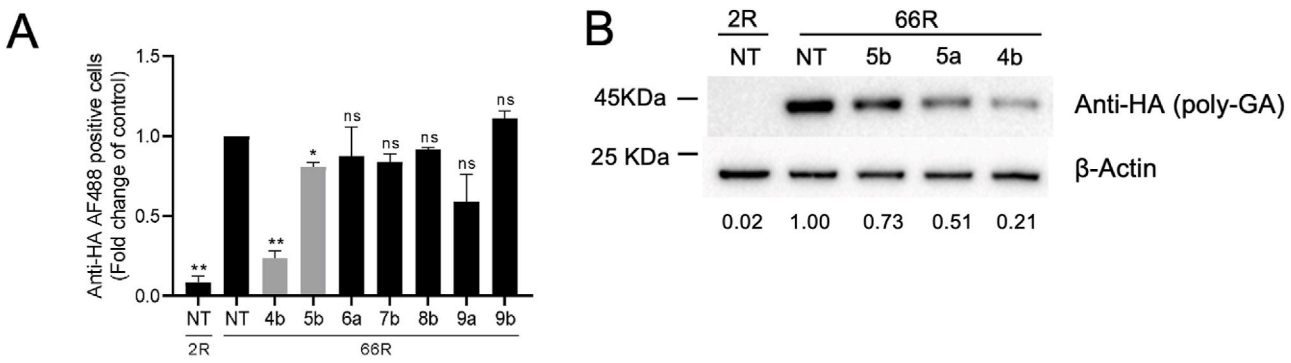

Fig. 4. Activity of (hetero)aryl di-GHs 4b - 9b on poly(GA) levels in 66R HEK293T cells. (A) Poly(GA) levels in cells transfected with either 2R (first bar, untreated/NT) and 66R plasmids (second to ninth bar) and treated for 24 h with (hetero)aryl di-GHs **4b**–**9b** (third to ninth bar) at sub-toxic concentrations (**4b**–20 μM; 5a – 15 μM; **5b**–1 μM: **6a** – 5 μM; **7b**–1 μM; **8b**–20 μM; **9a** – 20 μM; **9b**–7 μM). The gate for positive cells was defined using non-transfected cells. The percentage of positive cells was normalized to control (66R-transfected cells treated with DMSO – second bar). Biological triplicates were performed. The Welch's test was used to calculate statistical significance (ns-non-significant, *P < 0.05, **P < 0.01) between untreated/NT and **4b**–**9b** – tested 66R cells. (B) Immunoblotting analysis showing as heteroaryl di-GHs **4b**, **5a** and **5b** reduce poly-GA levels. β-actin was used as a loading control. Densitometric measurements of anti-HA (poly-GA) bands were normalized to β-actin levels for each tested small molecule. The obtained ratios were normalized to the control 66R NT. Data is presented as a fold-change to the control.

reductions in signal intensity in both the imino and aromatic regions of the spectra (Supplementary Fig. S2a and S2b), consistent with binding to the folded G4 RNA. Conversely, no significant spectral changes were observed in the hairpin-promoting buffer conditions (Supplementary Fig. S2c and S2d), suggesting that **4b** specifically recognizes the G4 conformation of the *C9orf72* RNA [23].

Molecular docking calculations were then performed to investigate the binding mode of **4b** to the G4 motif formed by the RNA G_4C_2 repeats in *C9orf72*. Since no experimental G4 structure for these RNA sequences is available either in the Protein Data Bank (PDB) or in other RNA structural databases, a recently developed G4 tridimensional model of the $(G_4C_2)_3GGGG$ RNA sequence was used [35]. This model shows a compact, parallel-stranded G4 structure featuring three stacked G-tetrads, three double-chain reversal loops, and wide stacking surfaces at the 5′ and 3′ ends. Thus, docking simulations were performed, encompassing the entire RNA structure. The majority of predicted docking poses (≈70 %) indicate that **4b** preferentially binds to the 3′ end of the G4 RNA, with its aromatic rings stacking upon the 3' G-tetrad and its GH branches forming hydrogen bonds with the sugar-phosphate backbone. The presence of multiple, albeit slightly different poses at this G4 region is probably due to the high symmetry of both **4b** and the nucleic acid structure. In the most representative, lowest energy pose (Fig. 9) the ligand engages in π–π stacking interactions with G3, G15 and G21, while its GH branches establish H-bonds with the phosphates of G2 and G20, and the N2 nitrogen of G21.

To further characterize the binding profile of **4b**, we examined its interaction with two additional G4 structures: the *c-kit2* promoter sequence (5′-d(CGGGCGGGCGCGAGGGAGGGG)-3′, PDB: 2KYP) [36], which adopts a parallel topology, and the thrombin-binding aptamer (TBA; 5′-d(GGTTGGTGTGGTTGG)-3′, PDB: 148D) [37], which folds into an antiparallel arrangement. In both cases, 1D ^{1}H NMR titrations revealed ligand-induced spectral changes both in the imino and aromatic proton regions, indicating possible binding to the folded G4 structures (Fig. S3). These findings suggest that **4b** would be capable of recognizing either parallel or antiparallel G4s, which is not uncommon among reported G4 ligands [6,38]. Notably, our hit GH **4b** maintains a clear preference for folded G4 motifs over non-G4 alternatives under the tested conditions. Altogether, these observations may inform future modifications aimed at enhancing topological or sequence selectivity towards the *C9orf72* RNA G-quadruplex.

3. Discussion and conclusions

Pathological, extended G_4C_2 repeats related to *C9orf72* mutations are clinically validated targets to fight an important fraction of ALS and FTD cases. G_4C_2 repeats' gain of toxicity is caused by a specific structural conformation acquired by the transcript, but also by the translation of this transcript into DPRs. Hence, targeting aberrant transcript could prevent G_4C_2 repeats toxicity *in toto*. Several ASOs showed a reduction of non-canonical RAN translation in clinical trials; although their development was halted due to adverse events, Phase I and II studies centered on ASOs and RNA interference acting on downstream pathways are either ongoing or planned on ALS patients with C*9orf72* mutation [20].

Small molecule RNA binders selective for extended G_4C_2 repeats progressed from early discovery to preclinical development; in particular, a tetracyclic piperazine showed specificity for the hairpin structure of $r(G_4C_2)_8$ constructs, reduced extended G_4C_2 repeats-dependent toxicity in c9ALS patient–derived stem cells and derived neurons, and showed *in vivo* efficacy by i.p. administration [35].

Bioavailability and *in vivo* potency are challenging goals for small molecule RNA binders, which contain flat aromatic cores to insert themselves between stacked base pairs, and polarized/protonated groups at physiological pH to interact with RNA phosphates [39]. We introduced guanyl hydrazones (GHs) as BBB-compliant decorations, ensuring a relevant percentage of neutral species at physiological pH; two GHs were either introduced on a bis thiophene *para* dinicotinimidamide RNA binding core or on similar scaffolds, to assemble an eight-membered array of putative RNA binders **4b-9b**.

Our array of (hetero)aryl di-GHs was profiled in an articulate set of cellular assays, including patient-derived progenitor and DPR-targeted mutated cells. Our aim was to find a suitable hit endowed with high tolerability, at least moderate potency, and better bioavailability due to GH substitutions; our active, bis-*para* and *meta* bis-thiophene(hetero) aryl di-GHs validated the amidine-GH switch, and expanded the activity-compatible structural diversity observed in diamidine **2b** with *meta* substitution patterns (**4b**, **5b**) and pyridine replacements (**4b**). Conversely, scaffold hopping with similar (bisoxazolephenyl **7a,b**) and more diverse cores (diphenyl urea diamides **8a,b**, phenyldioxy ditriazoles **9a,b**) led to inactive compounds. In particular, bis-thiophenepyridinyl *meta* diguanyl hydrazone **4b** showed good tolerability in wild-type HEK293T cells at micromolar concentrations.

Notably, **4b** is able to decrease poly(GA) levels in HEK293T cells expressing G_4C_2 66 repeats and poly(GP) aggregates levels in motor neuron-like NSC34 cells expressing the same repeat. These data were confirmed in patient-derived small molecule neural progenitor cells (smNPCs), where treatment with **4b** reduced poly(GA) levels. We then determined its selectivity in NSC34 cells transfected with individual tagged DPRs. Its sense-induced selectivity determined efficacy on sense

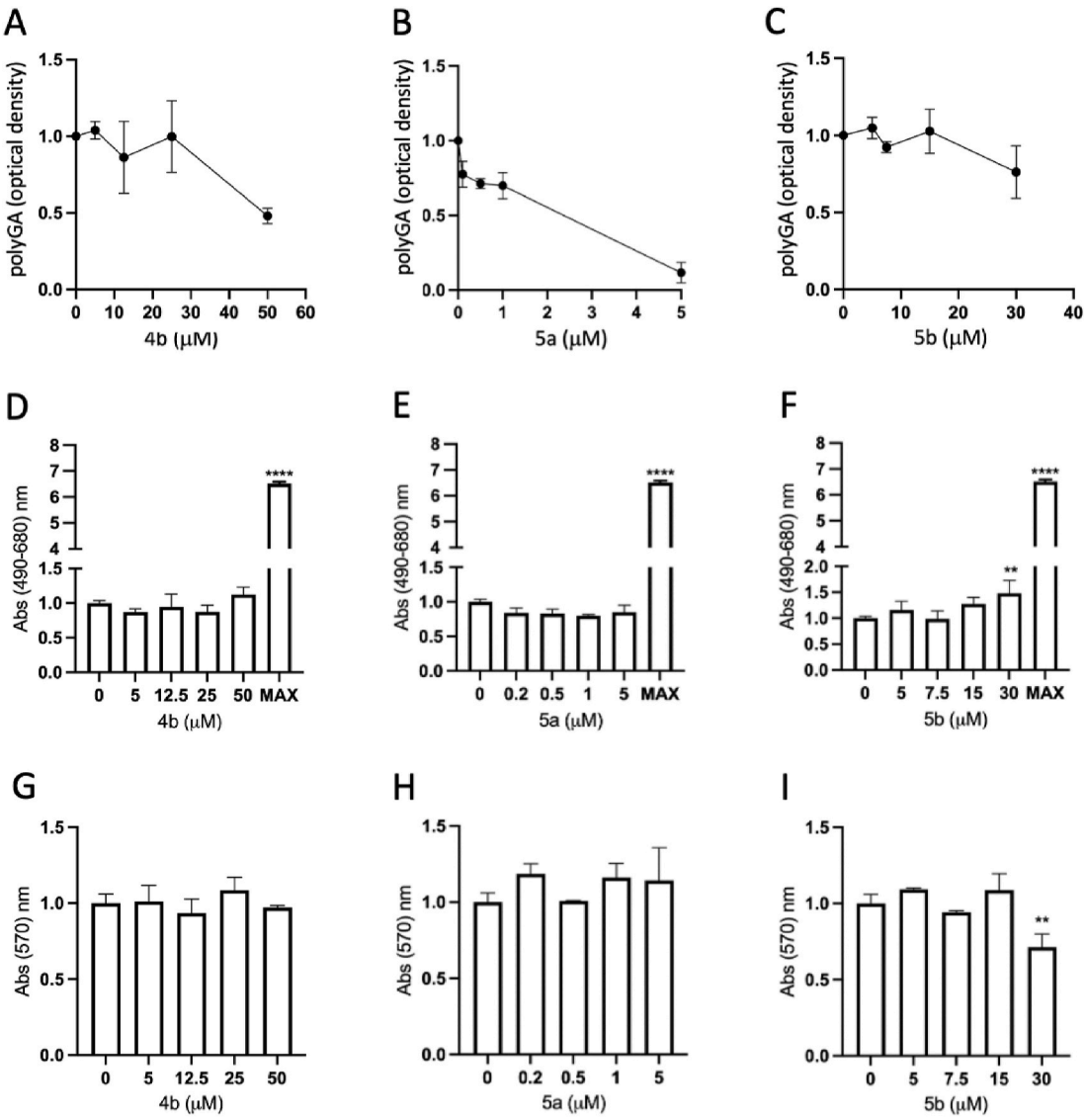

Fig. 5. Activity and tolerability of heteroaryl di-GHs 4b, 5a and 5b on poly(GA) levels in patient-derived smNPCs. smNPCs were treated for 24 h with four concentrations of **4b** (5; 12.5; 25; 50 μM, Panel A), **5a** (0.2; 0.5; 1; 5 μM, Panel B) or **5b** (5; 7.5; 15; 30 μM, Panel C). The bar graph represents the quantification of the immunoblot blot for poly(GA), whose values were normalized to the control (DMSO) condition. An LDH cytotoxicity assay was performed by treating cells exposed to the same testing concentrations with a lysis buffer, to evaluate the maximum LDH release (Panels D–F); LDH release values were normalized to the control (DMSO) condition (**$p < 0.005$, ****$p < 0.0001$, one-way ANOVA with Tukey's test). A cell viability MTT assay was performed by treating cells exposed to the same testing concentrations with MTT, and measuring MTT conversion to formazan by succinate dehydrogenase (Panels G–I); Formazan absorbance values at 570 nm wavelength were normalized to the control (DMSO) condition (**$p < 0.005$, one-way ANOVA with Tukey's test).

poly(GA) and poly(GP) repeats, while antisense poly(PR) levels were not affected. Moreover, **4b** did not affect target-unrelated β-galactosidase activity in transfected NSC34 cells.

Our combined NMR and docking data support the conclusion that **4b** binds to the G4 structure formed by the G_4C_2 repeat sequence in the *C9orf72* promoter, with no interaction detected when the RNA is folded into an alternative hairpin structure. Importantly, the ability of **4b** to target RNA G4s, and to discriminate between alternative RNA conformations, highlights its relevance as a G4 binder in a biological context where G4 folding is often transient or dynamic.

Additional binding studies with the *c-kit2* and TBA DNA G4s, which differ in topology and sequence, revealed that **4b** also engages structurally distinct G4s. While such recognition of different topologies is common among planar G4 ligands, the data suggest a scaffold-driven binding mode rather than non-specific affinity.

These evidences provide valuable hints for future optimization aimed at refining the ligand architecture to enhance selectivity for the *C9orf72* RNA G4 motif. Introducing asymmetry, by replacing one GH arm with a loop-interacting or polar side chain, could enhance recognition of the specific structural features of the targeted RNA motif. Likewise, incorporating conformational constraints through macrocyclization or intramolecular interactions may favor a pre-organized geometry better suited for selective stacking at defined G-tetrads. Once further improved the match of **4b** with the distinctive features of the *C9orf72* RNA G4, one might tune the charge distribution of **4b** to reduce the charge-driven binding with off-target nucleic acids. All these modifications may hopefully enable the development of more selective chemical probes for functional and therapeutic studies.

In conclusion, our data encourage us to further characterize heteroaryl di-GH **4b** *in vitro*, to study its impact on the progress of pathological cellular mechanisms, their rescue, and an increase in cell viability; and in pre-clinical studies, to assess its *in vivo* bioavailability and activity in C9-ALS mouse models. We will also focus on further structural optimization of **4b**, aiming to improve its potency by rational

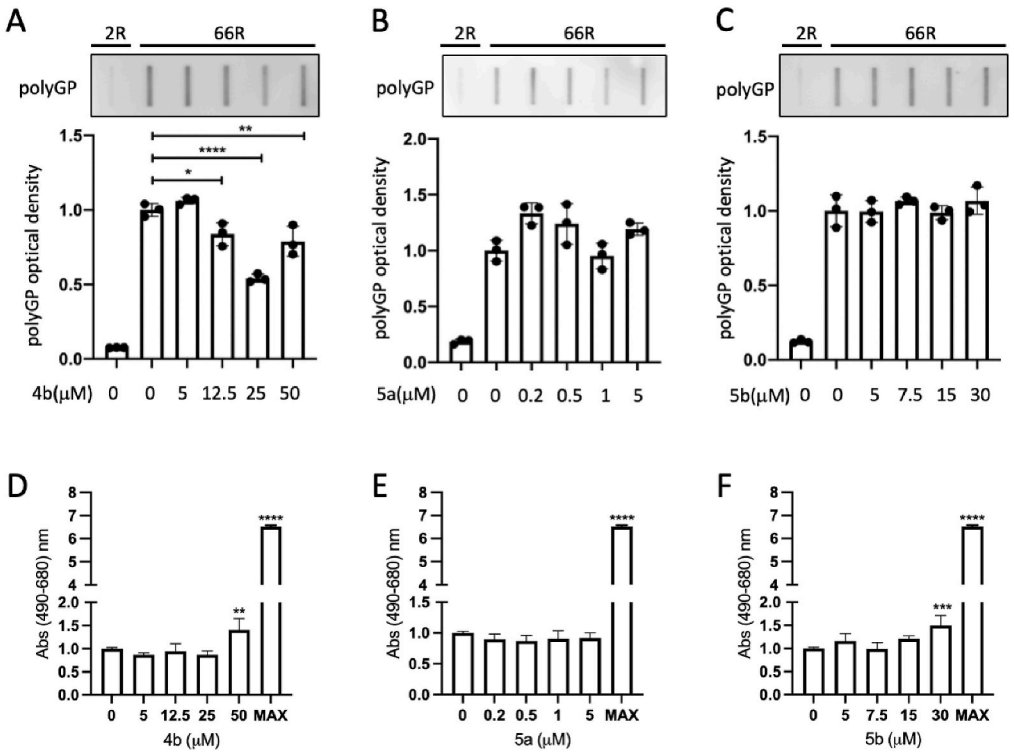

Fig. 6. Activity and tolerability of heteroaryl di-GHs 4b, 5a and 5b on poly(GP) levels in 66R NSC34 cells. NSC34 cells expressing the plasmids for either 2R (first lane) or 66R G_4C_2 were treated with four concentrations of **4b** (5; 12.5; 25; 50 μM, panel A), **5a** (0.2; 0.5; 1; 5 μM, panel B) or **5b** (5; 7.5; 15; 30 μM, panel C). The blot represents an FTA on poly(GP) high molecular weight species quantified in the graph (n = 3) (*p < 0.05, **p < 0.005, ****p < 0.0001, one-way ANOVA with Tukey's test). An LDH cytotoxicity assay was performed as described in Fig. 5, on NSC34 cells expressing the 66R G_4C_2 expansion (panels D–F); LDH release values were normalized to the control (DMSO) condition (**p < 0.005, ****p < 0.0001, one-way ANOVA with Tukey's test).

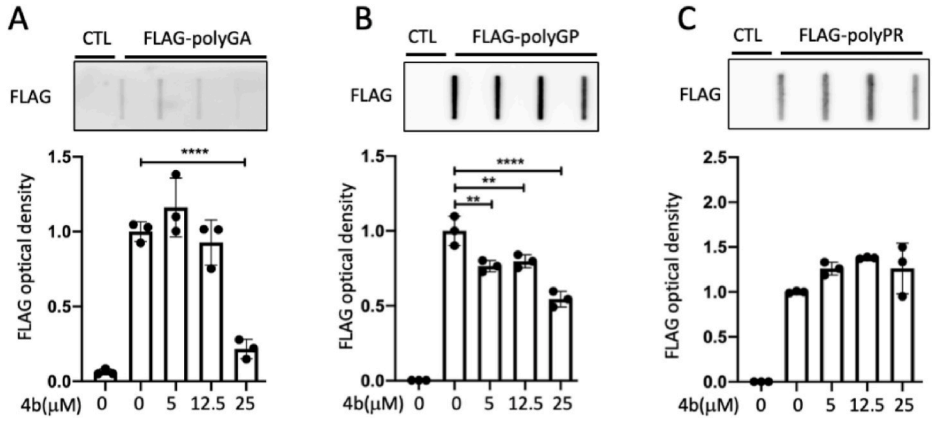

Fig. 7. Activity of hit heteroaryl di-GH 4b on poly(GA), (GP) and (PR) levels in poly(GA)-, poly(GP)- and poly(PR)overexpressing NSC34 cells. NSC34 cells expressing the plasmids for FLAG-tagged poly(GA) (panel A), poly(GP) (panel B) or poly(PR) (panel C) were treated with three safe concentrations of **4b** (5; 12.5; 25 μM). The blot represents an FTA on poly(GA) (A), poly(GP) (B) or poly(PR) (C) high molecular weight species quantified in the graph (n = 3) (**p < 0.005, ****p < 0.0001, one-way ANOVA with Tukey's test).

drug design.

4. Experimental section

4.1. Purity statement

Reaction intermediates and final synthetic targets were characterized by ^{1}H and ^{13}C NMR; such spectra, provided in the Supplementary Information, generally indicate a good purity. Aryl di-GHs **4b**–**9b** were run through an LC-MS purity check, confirming a ≥95 % purity suitable for biology profiling.

4.2. Synthesis

General Procedures. Oven-dried glassware was used to carry out chemical reactions, and dry solvents under a nitrogen atmosphere were employed. Solvents were purchased from Sigma Aldrich and used as such. Chemical reagents were purchased from Sigma Aldrich, Fluorochem and TCI. Purification of intermediates and final products was carried out by flash chromatography using high purity grade silica gel (Merck Grade, pore size 60 Å, 230–400 mesh particle size, Sigma-Aldrich, Milan, Italy) as a stationary phase. Alternatively, purification was performed by a BIOTAGE® system using Biotage Sfar Duo cartridges

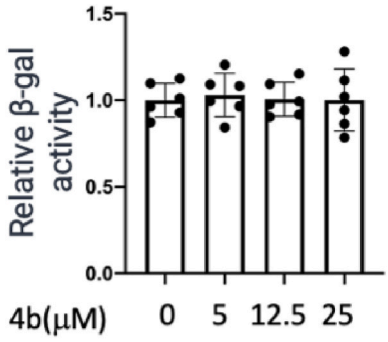

Fig. 8. Effects of heteroaryl di-GH 4b on β-galactosidase activity in β-galactosidase-overexpressing NSC34 cells. NSC34 cells expressing β-galactosidase were treated with **4b** (5; 12.5; 25 μM) in presence of the ONPG substrate. The bar graph represents the quantification of β-galactosidase activity.

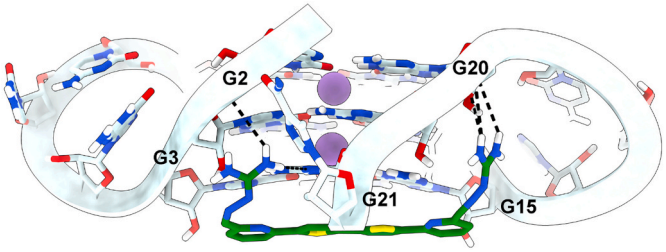

Fig. 9. Predicted binding mode of heteroaryl di-GH **4b** to the G4 RNA formed by the $(G_4C_2)_3GGGG$ repeat. The ligand is shown as green sticks, while the G4 structure is shown as light cyan cartoons. Metal ions are displayed as purple spheres. Hydrogen bonds are shown as dashed black lines. Docking simulations indicate preferential stacking at the 3′-end tetrad, with hydrogen bonding interactions between the ligand's GH arms and nearby phosphates. (For interpretation of the references to color in this figure legend, the reader is referred to the Web version of this article.)

(4, 10 or 25 g) for direct phase chromatography or Biotage Sfar Duo C_{18} cartridges (6, 12 or 30 g) for reverse phase chromatography. Reaction monitoring by thin layer chromatography (TLC) entailed Merck-precoated $60F_{254}$ plates, using UV light at 254 nm as a direct detection method, or by charring either with a phosphomolybdic acid ethanolic solution, with a potassium permanganate or a ninhydrin solution. ^{1}H NMR and ^{13}C NMR spectra were recorded in acetone-d_6, $CDCl_3$, CD_3OD, DMSO-d_6, or pyridine-d_5, depending on compounds' solubility, on Bruker DRX-400 or Bruker DRX-300 instruments. Chemical shifts (δ) for proton and carbon signals are quoted relatively to tetramethylsilane as an internal standard and expressed in parts per million (ppm). Ultra-high performance liquid chromatography/mass spectrometry analysis (UPLC/MS) was performed using an Acquity UPLC/MS System equipped with a tunable ultraviolet (TUV) detector, a single quadrupole (SQD) mass spectrometer and ACQUITY UPLC BEH SHIELD RP_{18} columns (2.1 × 100 mm, id = 1.7 μm).

*General method A for Suzuki coupling (***11b**, **12a**, **12b**, **13a***).* Bis-thiophene (1.0 eq) and a substituted 4-bromobenzaldehyde (2.0 eq) were introduced in two neck flasks under a N_2 atmosphere and dissolved in dry DMF. Then, solid K_2CO_3 (10.0 eq) and $Pd(PPh_3)_4$ (0.2 eq) were added to the solution. The resulting mixture was refluxed at 80 °C for 8 h, while monitored by TLC (eluent mixture: between 4.7:0.2:5 and 5:4:1 *n*-Hex/EtOAc/DCM). After reaction completion, the reaction mixture was cooled to room temperature and quenched with water. The aqueous phase was extracted with DCM (5 x 20 mL), the combined organic phases were washed with brine (10 mL), dried over anhydrous Na_2SO_4 and evaporated under reduced pressure. The crude was purified via direct flash column chromatography (eluent mixture: 5:1:4 *n*-Hex/EtOAc/DCM).

*General method B for guanyl hydrazone formation (***4b**, **5a**, **5b**, **7b**, **8b**, **9a**, **9b***).* AG.HCl (1.96 eq) was added to a vigorously stirred solution of dialdehyde (1 eq) in EtOH. A few drops of 1 M HCl were later added, the reaction mixture was stirred at reflux for 8 h and monitored by TLC (eluent mixture: 9:1 DCM/MeOH, developed in ninhydrin). After reaction completion, the reaction mixture was concentrated under reduced pressure obtaining a solid residue. The residue was triturated in DCM or Et_2O followed by filtration and, if necessary, a reverse phase chromatographic purification procedure.

6,6′-([2,2′-Bithiophene]-5,5′-diyl)dipicolinaldehyde **11b**: The reaction was performed according to general method A, using bis-thiophene bis-pinacol boronic ester (150 mg, 0.360 mmol, 1.0 eq), 6-bromopyridine 2-carboxaldehyde (138 mg, 0.740 mmol, 2.0 eq), dry DMF (18.0 mL), K_2CO_3 (498 mg, 3.60 mmol, 10.0 eq) and $Pd(PPh_3)_4$ (84 mg, 0.072 mmol, 0.2 eq). Pure dialdehyde **11b** (106 mg, 0.282 mmol, 78 % yield) was obtained as an orange solid. **^{1}H NMR (400 MHz, DMSO-d_6)** δ 10.00 (d, J = 1.0 Hz, 2H), 8.21 (dd, J = 8.0, 1.0 Hz, 2H), 8.08–8.04 (m, 2H), 7.89 (d, J = 4.0 Hz, 2H), 7.80 (dd, J = 8.0, 1.0 Hz, 2H), 7.50 (d, J = 4.0 Hz, 2H). **^{13}C NMR (101 MHz, DMSO-d_6)** δ 192.8, 152.0, 151.9, 142.3, 139.0, 138.4, 127.5, 125.6, 122.9, 119.9.

(2E,2′E)-2,2′-(([2,2′-bithiophene]-5,5′-diylbis(pyridine-6,2-diyl))bis (methaneylylidene))bis(hydrazone-1-carboximidamide) **4b**: The reaction was performed according to general method B, using dialdehyde **11b** (35 mg, 0.093 mmol, 1.0 eq), AG.HCl (20 mg, 0.182 mmol, 1.96 eq) and EtOH (4.65 mL). Pure target **4b** was obtained as an orange solid (48 mg, 0.085 mmol, 92 % yield) after cooling, filtration of the precipitate and drying. **MS (ESI$^+$):** m/z $[M + H]^+$ 489.35; calculated MS for $C_{22}H_{21}N_{10}S_2$: 489.14. **^{1}H NMR (400 MHz, DMSO-d_6)** δ 12.51 (s, 2H), 8.20 (s, 2H), 8.18 (dd, J = 8.0, 1.1 Hz, 2H), 8.01 (dd, J = 8.0, 1.1 Hz, 2H), 7.95 (t, J = 8.0 Hz, 2H), 7.86 (d, J = 4.0 Hz, 2H), 7.51 (d, J = 4.0 Hz, 2H). **^{13}C NMR (101 MHz, DMSO-d_6)** δ 155.4, 152.2, 151.3, 146.4, 142.9, 138.6, 137.8, 127.0, 125.8, 119.5, 119.1.

4.3. Biological profiling

4.3.1. Cell cultures

HEK293T cells were obtained from American Type Culture Collection (ATCC) and cultured in Dulbecco's modified Eagle's medium - DMEM (Gibco) supplemented with 10 % fetal bovine serum (FBS), 2 mM L-glutamine, and 100 U/mL penicillin-streptomycin (all from Lonza). Cells were maintained at 37 °C under humidified conditions with 5 % CO_2.

CS52iALS-C9n6 (RRID:CVCL JC27) and CS52iALS-C9n6.ISOC3 iPSC lines were bought from Cedars-Sinai Medical Center iPSC Core Facility, Los Angeles, USAsts. iPSCs were cultured on Matrigel (Corning, 354277) and fed with E8 (ThermoFisher Scientific, A1517001). Every 5–6 days, cells were split using Accutase (Merck, A6964), and in the first day, E8 was supplemented with ROCK-I (5 μM; Selleckchem, S1049).

4.3.2. Cellular viability assay

HEK293T cells were seeded in 96 well plates at a confluence of 120,000 cells/mL in 100 μL (12,000 cells/well). The following day, cells were treated with increasing concentrations (0; 0.3125; 0.625; 1.25; 2.5; 5; 10; 20; 40 μM) of each (hetero)aryl di-GH **4b**–**9b**. After 24 h of treatments, cells were incubated with 10 μL of OzBlue reagent (OzBiosciences). The fluorescence signal (560/590 nm) was assessed after 2 h of incubation using the Varioskan LUX Multimode Microplate Reader (Thermo Scientific) according to the manufacturer instructions. Each analysis was performed in triplicate, and the average signal normalized to the DMSO control treatment (0.01 %).

4.3.3. Cytotoxicity (LDH) assay – HEK293T, smNPC and NS34 cells

As to HEK293T cells, they were seeded in 96 well plates at a confluence of 120,000 cells/mL in 100 μL (12,000 cells/well). The following day, cells were treated with test concentration of the (hetero)

aryl di-GH **4b**–**9b** (**4b**–20 μM; **5a** – 15 μM; **5b**–1 μM; **6a** – 5 μM; **7b**–1 μM; **8b**–20 μM; **9a** – 20 μM; **9b**–7 μM). Cells were also treated with the apoptosis inducer staurosporine (2 μM) for 2 h. Following 24 h of exposure to test compounds, 50 μL of supernatant was transferred to a transparent 96 well plate and lactate dehydrogenase (LDH) release was quantified, following the manufacturer's protocol (Pierce LDH Cytotoxicity Assay Kit, 88953, Thermo Scientific). In details, supernatants were incubated with an equal volume of reaction mixture containing the substrate mix and the assay buffer. After 30 min of incubation at room temperature, the reaction was stopped with 50 μL of stop solution. The absorbance values at 490 nm (LDH release) and 680 nm (background signal from the instrument) were measured using the Varioskan LUX Multimode Microplate Reader (Thermo Scientific). Data are presented as a difference between the absorbance values at 490 nm and 680 nm. Each condition was performed in triplicate, and the average signal normalized to the DMSO control treatment (0.01 %).

As to smNPCs and NSC34 cells, the CyQUANT™ LDH Cytotoxicity Assay Kit (Thermo Fisher Scientific, C20301) was used. Cells were treated for 24 h with different concentrations of heteroaryl di-GHs **4b**, **5a** and **5b**, as reported in the legend of Figs. 5 and 6. As a positive control, the maximum LDH release was measured on cells incubated with a lysis buffer for 45 min at 37°. The test was then performed on 50 μL of supernatant, following the manufacturer's protocol. The absorbance was measured at 490 nm and 680 nm wavelengths, using an Enspire® Multimode Plate Reader (PerkinElmer, Inc., Waltham, MA, USA). Each test condition was performed in quadruplicate, and the average signal was normalized to the DMSO control treatment.

4.3.4. Cytotoxicity (MTT) assay - smNPCs

The 3-(4,5-dimethyl-2-thiazolyl)-2,5 diphenyl-2H-tetrazolium bromide (MTT; Sigma-Aldrich, M2128)-based cell proliferation assay (MTT assay) was performed on smNPCs after 24 h of treatment with heteroaryl di-GHs **4b**, **5a** and **5b** at selected concentrations, in MW24 plates seeded at 150,000 cell/mL. Then, the culture medium was removed, and cells were incubated with MTT solution (1.5 mg/mL in N2B27) at 37 °C for 30 min; then, isopropanol was added to block the reaction and solubilize the precipitates. The absorbance of each well was measured at 570 nm wavelength, using an Enspire® Multimode plate reader (PerkinElmer, Waltham, MA, USA).

4.3.5. Primary screening – Poly-GA levels

HEK293T cells were seeded in 24 well plates at a confluence of 200,000 cells/mL in 1 mL (200,000 cells/well). The following day, cells were transfected with 1 μg of constructs containing either two (2R) or sixty-six (66R) G_4C_2 repetitions. Transfection was performed using Lipofectamine 3000 (Life Technologies), according to the manufacturer instructions. Cells were treated with the selected test concentrations for each (hetero)aryl di-GH **4b**–**9b** at the time of transfection. Following 24 h of transfection/treatment, cells were collected and fixed for 8 min with 4 % aqueous paraformaldehyde (Sigma Aldrich). After being washed twice with PBS, cells were permeabilized for 8 min with a 90 % methanol solution in PBS, followed by centrifugation at 2400 rpm for 3 min to remove the permeabilization solution. Cells were then blocked for 30 min with 5 % BSA and incubated for 1 h with a solution containing an anti-HA Tag monoclonal antibody conjugated with Alexa Fluor™ 488 (Anti-HA AF488 - Life Technologies), at 1:100 concentration in 0.5 % BSA. Cells were washed and analyzed using a Symphony A1 flow cytometer (BD Biosciences). Non-transfected cells were used to discriminate between negative and AF488 positive populations, for all tested di-GHs except yellow-colored **4b**. Given its interference with the AF488 fluorophore, the negative population for the latter was defined with HEK293T cells transfected with the 66R plasmid and treated with **4b**, avoiding incubation with Anti-HA AF488. The percentage of AF488 positive cells was quantified using the BD FACSDiva™ Software.

4.3.6. Hit validation - protein extraction and immunoblotting

HEK293T cells were transfected and treated with heteroaryl di-GHs **4b**, **5a** and **5b** at selected test concentrations, as previously described for the primary screening. Samples were then lysed on ice with RIPA lysis buffer supplemented with Protease Inhibitor Cocktail (ThermoScientific) for 10 min. The protein lysate was quantified using the BCA method (Life Technologies), accordingly with the manufacturer's instructions. The same amount of protein was loaded into a 15 % SDS-polyacrylamide gel. Following protein transfer to a PVDF membrane and blocking with a 5 % BSA solution, the membrane was incubated with Anti-HA (Bethyl A190-108A; Dilution 1: 1000). β-actin (BK4970S CST; 1:3000 dilution) was used as a protein loading control. An anti-rabbit secondary antibody (111-035-003; 1:5000 dilution) was used and obtained from Jackson Immunoresearch Laboratories. Protein signals were revealed at ChemiDoc (BioRad) with chemiluminescence detection kit reagents (Amersham ECL Select, GE Healthcare). The relative density of protein bands was analyzed using the ImageJ software (Opensource, https://imagej.net/ij/download.html), and represented as the fold change of the 66R non-treated control. A representative Western blot of three independent biological experiments is shown.

4.3.7. iPSC differentiation

iPSCs were differentiated into smNPCs following a published protocol [40]. In brief, embryo bodies were derived from iPSCs and maintained in a N2B27 medium composed of DMEM HAM'S F-12 (Euroclone, ECM0090L), Neurobasal medium (ThermoFisher Scientific, 21103049), N-2™ supplement (ThermoFisher Scientific, 17502048), B-27™ supplement (ThermoFisher Scientific, 17504044) and 1 % penicillin/streptomycin/glutamine. Cells were treated with CHIR-99021 (Axon MedChem), SB-431542 (Ascent Scientific), LDN 193189 (Tocris Bioscience), Smoothened Agonist SAG (STEMCELL Technologies) and ascorbic acid AA (SigmaAldrich). After 6 days, embryo bodies were dissociated and plated on Matrigel (hESC-qualified Matrix; Corning®, 354277) in a medium composed of N2B27 with CHIR, AA, and SAG. smNPCs were cultured for 6–7 passages before performing experiments. smNPCs were plated with 150,000 cell/mL density and were treated with different concentrations of heteroaryl di-GHs **4b**, **5a** and **5b** as reported in the figure legend.

4.3.8. Immunodot – blot assay

Poly-GA levels were analyzed with an Immunodot - blot assay. smNPCs were collected and centrifuged at 1200 rpm for 5 min at 4 °C. Cell pellets were resuspended in phosphate-buffered saline (PBS; Sigma-Aldrich, P4417) supplemented with Protease Inhibitor Cocktail (Sigma-Aldrich, P8340), and an ultrasonic homogenization was performed. The protein concentration was quantified with the BCA method, using a Quantum Protein Assay Kit (CYANAGEN PRTD1, 0500). 6 μg of total proteins were concentrated on a 0.22 μm nitrocellulose membrane (Whatman GE Healthcare, GEH10404180) using a Bio-Dot SF Microfiltration Apparatus (Bio-Rad Laboratories, 1703938). Membranes were then blocked with 10 % no-fat milk in Tris-buffered saline with 0.01 % Tween (TBS-T), and subsequently incubated overnight at 4 °C with an anti-GA (Millipore; MABN889) (1:1000 dilution) antibody, and then for 1 h at room temperature with a goat anti-mouse IgG-HRP (Jackson ImmunoResearch, 115–035-003) (1:5000 dilution).

4.3.9. NSC34 cultures and transfection

The mouse motoneuron-like hybrid cell line NSC34 [41] was cultured in DMEM high-glucose medium (EuroClone, ECB7501L) supplemented with 5 % fetal bovine serum (Sigma-Aldrich, F7524), 1 mM L-glutamine (EuroClone, ECB3004D), and penicillin-streptomycin solution (Euroclone, ECB3001D), and was then grown at 37 °C in 5 % CO_2. NSC34 cells were plated with an 80,000 cells/mL density and were transfected with 1 μg of DNA plasmid using Lipofectamine 3000® (ThermoFisher Scientific, L3000015). As reported in the figure legend,

NSC34 cells were treated with different concentrations of selected heteroaryl di-GHs **4b**, **5a**, and **5b**.

pAG3-CAG-(G_4C_2)x2 or (G_4C_2)x66 (2R or 66R) vectors were used for transfection and testing with heteroaryl di-GH **4b**. Both constructs contain the native intronic sequence above the repeat. FLAG-tagged plasmids coding for scrambled-GA, scrambled-GP, and scrambled-PR (100 repeats) were kindly provided by Prof. Daisuke Ito (Keio University School of Medicine, Tokyo, Japan). These plasmids were optimized to encode for the single evaluated DPRs. Finally, the pCMV-β-galactosidase plasmid was used for transfection and testing with **4b**.

4.3.10. Filter trap assay

To evaluate the activity of tested compounds on selected DPRs, a Filter trap assay (FTA) was used. NSC34 cells were collected as described for smNPCs. 6 μg of total proteins were filtered on a 0.22 μm cellulose acetate membrane (Whatman GE Healthcare, GEH10404180), using a Bio-Dot SF Microfiltration Apparatus (Bio-Rad Laboratories, 1703938). Membranes were analyzed as described for the immunodot-blot. An anti-FLAG (Sigma-Aldrich, F1804) was used as primary antibody, and a goat anti-mouse IgG-HRP (Jackson ImmunoResearch, 115–035-003) (1:5000 dilution) was used as a secondary antibody.

4.3.11. β-galactosidase assay

To evaluate β-galactosidase activity in NSC34 cells, a solution (4 mg/mL) of its ortho-nitrophenyl-β-galactoside (ONPG) substrate was added to cell lysates. After 30 min of incubation at 37 °C, absorbances at 420 nm were measured using an Enspire® Multimode plate reader (PerkinElmer, Waltham, MA, USA).

4.4. Biophysical studies

4.4.1. RNA and DNA oligonucleotide sample preparation and annealing

An HPLC-purified RNA oligonucleotide with the sequence $(G_4C_2)_8$, and two DNA oligonucleotides with sequence 5′-d(CGGGCGGGCGCGAGGGAGGGG)-3′ from the c-kit2 gene promoter and sequence 5′-d(GGTTGGTGTGGTTGG)-3′ corresponding to the thrombin-binding aptamer (TBA) were purchased from Dharmacon. Oligonucleotides were supplied as a lyophilized powder and reconstituted in ultrapure water to a 5 mM stock concentration. Annealing was performed by heating the samples to 90 °C, followed by gradual cooling to room temperature overnight. For RNA hairpin folding, annealing was carried out in the presence of 100 mM NaCl and 10 mM potassium phosphate buffer at pH 7.0. For RNA and DNA quadruplex formation, annealing was conducted in 100 mM KCl and 10 mM Tris buffer at pH 7.0.

4.4.2. NMR spectroscopy

NMR experiments were conducted on a Bruker Avance NEO 700 MHz spectrometer equipped with a Z-gradient cryoprobe. Data acquisition and processing were performed using the Bruker TOPSPIN 4.1.3 software suite. One-dimensional ^{1}H NMR spectra were recorded at 25 °C with a spectral width of 26 ppm, 2048 scans, and a relaxation delay of 2 s. RNA and DNA samples were prepared in 10 % D_2O and 90 % H_2O. Spectra were acquired using a 1:4 nucleic acid/ligand concentration ratio. NMR spectra obtained for *C9orf72* RNA structures in hairpin and quadruplex conformations, and TBA and *c-kit2* DNA G4s are consistent with data reported in literature [22,34,36,37].

4.5. Molecular modeling

4.5.1. Molecular docking

The tridimensional model of the RNA G-quadruplex formed by the $(G_4C_2)_3$GGGG sequence [35] was kindly provided by Prof. Chen Wu (College of Science and Mathematics, Rowan University, Glassboro, New Jersey 08028, United States). This structure was prepared using the Protein Preparation Wizard [42] in Maestro [43], version 13.5. Missing hydrogen atoms were added. Protonation states and hydrogen bonding networks at local pH were assigned using the PropKa program [44] included in Maestro [42]. Finally, the positions of all the hydrogens were minimized.

Heteroaryl di-GH **4b** was designed using the 2D Sketcher tool in Maestro [43] and subsequently prepared with the LigPrep module [45], using the OPLS4 force field [46]. The ligand's tautomeric and protonation state in the interval pH 7.0 ± 1.5 were assigned using Epik [47].

Docking calculations were performed with the grid-based program Glide (v. 9.8) [48]. For grid generation, we used the Receptor Grid Generation tool implemented in Glide [48]. The docking search area was set large enough to include the whole G4 structure, with an inner box measuring 14 Å × 14 Å × 14 Å and an outer box measuring 34 Å × 34 Å × 34 Å. Docking was performed in the standard precision (SP) mode [49,50] and using the OPLS2005 force field. Otherwise, default parameters were applied. The top 50 poses were selected for post-docking minimization, after which the 20 best poses were retained as the final output.

CRediT authorship contribution statement

Alice Maiocchi: Writing – review & editing, Methodology, Investigation, Conceptualization. **Martina Pedrini:** Writing – review & editing, Methodology, Investigation, Conceptualization. **Veronica Ferrari:** Writing – review & editing, Methodology, Investigation. **Agata Sofia Assunçao Carreira:** Writing – review & editing, Methodology, Investigation, Conceptualization. **Vincenzo Maria D'Amore:** Writing – review & editing, Methodology, Investigation, Conceptualization. **Federica Santoro:** Methodology, Investigation. **Anna Di Porzio:** Investigation. **Maddalena Bosetti:** Methodology, Investigation. **Riccardo Cristofani:** Writing – review & editing, Methodology, Investigation, Conceptualization. **Alessandra Silvani:** Supervision, Conceptualization. **Diego Brancaccio:** Writing – review & editing, Methodology, Investigation, Conceptualization. **Luciana Marinelli:** Writing – review & editing, Supervision, Conceptualization. **Francesco Saverio Di Leva:** Writing – review & editing, Supervision, Methodology, Conceptualization. **Alessandro Provenzani:** Writing – review & editing, Supervision, Methodology, Conceptualization. **Angelo Poletti:** Writing – review & editing, Supervision, Methodology, Conceptualization. **Pierfausto Seneci:** Writing – original draft, Supervision, Project administration, Methodology, Conceptualization.

Declaration of competing interest

The authors declare that they have no known competing financial interests or personal relationships that could have appeared to influence the work reported in this paper.

Acknowledgments

This research was funded by Fondazione Telethon - Italy (n. GGP19128 to AP), Association Française contre les Myopathies - France (AFM Telethon n. 23236 to 1295 AP), and Ministero dell'Università e della Ricerca (MIUR) – Italy (PRIN—Progetti di ricerca di interesse nazionale (n. 2017F2A2C5 to AP); CN3: RNA – Codice Proposta: CN_00000041; Tematica Sviluppo di terapia genica e farmaci con tecnologia a RNA (Centro Nazionale di Ricerca – CN3 National Center for Gene Therapy, and Drugs based on RNA Technology to AP, LM, FSDL, DP, ADP and VMDA); Progetto Dipartimenti di Eccellenza to DiSFeB); BaC CN RNA & GT Spoke 3 – PNRR - M4C2 INV 1.4 "RNA-based Approaches for Precision Intervention in neurologic Diseases (RAPID)" (CN00000041 – CUP J63C24000100007) to APr; Progetto Dipartimenti di Eccellenza to DeCIBIO (University of Trento).

The authors thank Prof. Chun Wu from Rowan University (USA) for providing the tridimensional G-quadruplex model used for computational studies.

Appendix A. Supplementary data

Supplementary data to this article can be found online at https://doi.org/10.1016/j.ejmech.2025.117736.

Abbreviations used

AG.HCl, aminoguanidine hydrochloride; ALS, amyotrophic lateral sclerosis; ASO, antisense oligonucleotide; BBB, blood brain barrier; CNS, central nervous system; DMF, dimethylformamide; DMSO, dimethyl sulfoxide; DPR, dipeptide protein repeat; ESI, electrospray ionization, EtOAc, ethyl acetate; FTA, filter trap assay; FTD, frontotemporal dementia; GH, guanyl hydrazone; HPLC, high performance liquid chromatography; i.p, intraperitoneal; MeOH, methanol; MS, mass spectrometry; NMR, nuclear magnetic resonance; NPC, nuclear pore complex; poly(GA), PNS, peripheral nervous system; polyGlycineAlanine; poly(GP), polyGlycineProline; poly(GR), polyGlycineArginine; poly(PR), polyProlineArginine; poly(PA), polyProlineAlanine; RAN, repeat associated non-AUG dependent; siRNA, short interfering RNA; smNPC, small molecule neural progenitor cell; SP, standard precision; THF, tetrahydrofuran.

Data availability

Data will be made available on request.

References

[1] C.H. Jones, J.R. Androsavich, N. So, M.P. Jenkins, D. MacCormack, A. Prigodich, V. Welch, J.M. True, M. Dolsten, Breaking the mold with RNA- a "RNAissance" of life science, npj Genom. Med. 9 (2024) 2, https://doi.org/10.1038/s41525-023-00387-4.

[2] Y. Zhu, L. Zhu, X. Wang, H. Jin, RNA-Based therapeutics: an overview and prospectus, Cell Death Dis. 13 (2022) 644, https://doi.org/10.1038/s41419-022-05075-2.

[3] K. Paunovska, D. Loughrey, J.D. Dahiman, Drug delivery systems for RNA therapeutics, Nat. Rev. Genet. 23 (2022) 265–280, https://doi.org/10.1038/s41576-021-00439-4.

[4] K.M. Krause, A.W. Serio, T.R. Kane, L.E. Connolly, Aminoglycosides: an overview, Cold Spring Harb. Perspect. Med. 6 (2016) a027029, 10.1101%2Fcshperspect.a027029.

[5] H. Ratni, R.S. Scalco, A.H. Stephan, Risdiplam, the first approved small molecule splicing modifier drug as a blueprint for future transformative medicines, ACS Med. Chem. Lett. 12 (2021) 874–877, https://doi.org/10.1021/acsmedchemlett.0c00659.

[6] J.L. Childs-Disney, X. Yang, Q.M.R. Gibaut, Y. Tong, R.T. Bate, M.D. Disney, Targeting RNA structures with small molecules, Nat. Rev. Drug Discov. 21 (2022) 736–762, https://doi.org/10.1038/s41573-022-00521-4.

[7] B.S. Morgan, J.E. Forte, R.N. Culver, Y. Zhang, A.E. Hargrove, Discovery of key physicochemical, structural, and spatial properties of RNA-targeted bioactive ligands, Angew. Chem. Int. Ed. 56 (2017) 13498–13502, https://doi.org/10.1002/anie.201707641.

[8] W.J. Martin, P. Grandi, M. Marcia, Screening strategies for identifying RNA- and ribonucleoprotein-targeted compounds, Trends Pharmacol. Sci. 42 (2021) 758–771, https://doi.org/10.1016/j.tips.2021.06.001.

[9] R. Bose, F. Irfana, A.M. Mustoe, Causes, functions, and therapeutic possibilities of RNA secondary structure ensembles and alternative states, Cell Chem. Biol. 31 (2024) 17–35, https://doi.org/10.1016/j.chembiol.2023.12.010.

[10] S.P. Velagapudi, S.M. Gallo, M.D. Disney, Sequence-based design of bioactive small molecules that target precursor microRNAs, Nat. Chem. Biol. 10 (2014) 291–297, https://doi.org/10.1038/nchembio.1452.

[11] F.P. Panei, R. Torchet, H. Menager, P. Gkeka, M. Bonomi, HARIBOSS: a curated database of RNA-Small molecules structures to aid rational drug design, Bioinformatics 38 (2022) 4185–4193, https://doi.org/10.1093/bioinformatics/btac483.

[12] R.H. Brown, A. Al-Chalabi, Amyotrophic lateral sclerosis, N. Engl. J. Med. 377 (2017) 162–172, https://doi.org/10.1056/nejmra1603471.

[13] S. Ajroud-Driss, T. Siddique, Sporadic and hereditary amyotrophic lateral sclerosis (ALS), Biochim. Biophys. Acta 1852 (2015) 679–684, https://doi.org/10.1016/j.bbadis.2014.08.010.

[14] H. Sivasathiaseelan, C.R. Marshall, J.L. Agustus, E. Benhamou, R.L. Bond, J.E. P. van Leeuwen, C.J.D. Hardy, J.D. Rohrer, J.D. Warren, Frontotemporal dementia: a clinical review, Semin. Neurol. 39 (2019) 251–263, https://doi.org/10.1055/s-0039-1683379.

[15] D.W. Sirkis, E.G. Geier, L.W. Bonham, C.M. Karch, J.S. Yokoyama, Recent advances in the genetics of frontotemporal dementia, Curr. Genet. Med. Rep 7 (2019) 41–52, https://doi.org/10.1007/s40142-019-0160-6.

[16] M. DeJesus-Hernandez, I.R. Mackenzie, B.F. Boeve, A.L. Boxer, M. Baker, N. J. Rutherford, A.M. Nicholson, N.A. Finch, H. Flynn, J. Adamson, N. Kouri, A. Wojtas, P. Sengdy, G.-Y.R. Hsiung, A. Karydas, W.W. Seeley, K.H. Josephs, G. Coppola, D.H. Geschwind, Z.K. Wszolek, H. Feldman, D.S. Knopman, R. C. Petersen, B.L. Miller, D.W. Dickson, K.B. Boylan, N.R. Graff-Radford, R. Rademakers, Expanded GGGGCC hexanucleotide repeat in noncoding region of C9ORF72 causes chromosome 9p-linked FTD and ALS, Neuron 72 (2011) 245–256, https://doi.org/10.1016/j.neuron.2011.09.011.

[17] A.N. Coyne, B.L. Zaepfel, L. Hayes, B. Fitchman, Y. Salzberg, E.-C. Luo, Bowen, H. Trost, S. Aigner, F. Rigo, G.W. Yeo, A. Harel, C.N. Svendsen, D. Sareen, J. D. Rothstein, G4C2 repeat RNA initiates a POM121-Mediated reduction in specific nucleoporins in C9orf72 ALS/FTD, Neuron 107 (2020) 1124–1140, https://doi.org/10.1016/j.neuron.2020.06.027.

[18] W. Pang, F. Hu, Cellular and physiological functions of C9ORF72 and implications for ALS/FTD, J. Neurochem. 157 (2022) 334–350, https://doi.org/10.1111/jnc.15255.

[19] R. Balendra, A.M. Isaacs, *C9orf72*-mediated ALS and FTD: multiple pathways to disease, Nat. Rev. Neurol. 14 (2018) 544–558, https://doi.org/10.1038/s41582-018-0047-2.

[20] R. Sattler, B.J. Traynor, J. Robertson, L. Van Den Bosch, S.J. Barmada, C. N. Svendsen, M.D. Disney, T.F. Gendron, P.C. Wong, M.R. Turner, A. Boxer, S. Babu, M. Benatar, M. Kurnellas, J.D. Rohrer, C.J. Donnelly, L.M. Bustos, K. Van Keuren-Jensen, P.A. Dacks, M.N. Sabbagh, Roadmap for C9ORF72 in frontotemporal dementia and amyotrophic lateral sclerosis: report on the C9ORF72 FTD/ALS summit, Neurol. Ther. 12 (2023) 1821–1843, https://doi.org/10.1007/s40120-023-00548-8.

[21] K.E. Meijboom, R.H. Brown, Approaches to gene modulation therapy for ALS, Neurotherapeutics 19 (2022) 1159–1179, https://doi.org/10.1007/s13311-022-01285-w.

[22] A. Ursu, J.T. Baisden, J.A. Bush, A. Taghavi, S. Choudhary, Y.-J. Zhang, T. F. Gendron, L. Petrucelli, I. Yildirim, M.D. Disney, A small molecule exploits hidden structural features within the RNA repeat expansion that causes c9ALS/FTD and rescues pathological hallmarks, ACS Chem. Neurosci. 12 (2021) 4076–4089, https://doi.org/10.1021/acschemneuro.1c00470.

[23] A. Cheng, C. Liu, W. Ye, D. Huang, W. She, X. Liu, C.P. Fung, N. Xu, M.C. Suen, W. Ye, H.H.Y. Sung, I.D. Williams, G. Zhu, P.Y. Qian, Selective *C9orf72* G-Quadruplex-Binding small molecules ameliorate pathological signatures of ALS/FTD models, J. Med. Chem. 5 (2022) 12825–12837, https://doi.org/10.1021/acs.jmedchem.2c00654.

[24] F.J. Groelly, M. Porru, J. Zimmer, H. Benainous, Y. De Visser, A.A. Kosova, S. Di Vito, V. Serra, A. Ryan, C. Leonetti, A. Bruna, A. Biroccio, M. Tarsounas, Anti-tumoural activity of the G-quadruplex ligand pyridostatin against BRCA1/2-deficient tumours, EMBO Mol. Med. 14 (2022) e14501, https://doi.org/10.15252/emmm.202114501.

[25] R. Simone, R. Balendra, T.G. Moens, E. Preza, K.M. Wilson, A. Heslegrave, N. S. Woodling, T. Niccoli, J. Gilbert-Jaramillo, S. Abdelkarim, E.L. Clayton, M. Clarke, M.T. Konrad, A.J. Nicoll, J.S. Mitchell, A. Calvo, A. Chio, H. Houlden, J. M. Polke, M.A. Ismail, C.E. Stephens, T. Vo, A.A. Farahat, W.D. Wilson, D. W. Boykin, H. Zetterberg, L. Partridge, S. Wray, G. Parkinson, S. Neidle, R. Patani, P. Fratta, A.M. Isaacs, G-quadruplex-binding small molecules ameliorate c9orf72 FTD/ALS pathology in vitro and in vivo, EMBO Mol. Med. 10 (2018) 22–31, https://doi.org/10.15252/emmm.201707850.

[26] L. Muzio, R. Sirtori, A. Fossaghi, D. Gornati, S. Eleuteri, D. Brancaccio, L. Manzoni, L. Ottoboni, L. De Feo, A. Quattrini, E. Mastrangelo, L. Sorrentino, E. Scalone, G. Comi, L. Marinelli, N. Riva, M. Milani, P. Seneci, G. Martino, Therapeutic effects of retromer stabilization in Amyotrophic lateral sclerosis models, Nat. Commun. 11 (2020) 3848, https://doi.org/10.1038/s41467-020-17524-7.

[27] D. Gornati, R. Ciccone, A. Vinciguerra, S. Ippati, A. Pannaccione, T. Petrozziello, E. Pizzi, A. Hassan, E. Colombo, S. Barbini, M. Milani, C. Caccavone, P. Randazzo, L. Muzio, L. Annunziato, A. Menegon, A. Secondo, E. Mastrangelo, G. Pignataro, P. Seneci, Synthesis and characterization of novel mono- and bis-guanylhydrazones as potent and selective ASIC1 inhibitors able to reduce brain ischemic insult, J. Med. Chem. 64 (2021) 8333–8353, https://doi.org/10.1021/acs.jmedchem.1c00305.

[28] S.S. Chourasiya, D. Kathuria, S.S. Nikam, A. Ramakrishnan, S. Khullar, S. K. Mandal, A.K. Chakraborti, P.V. Bharatam, Azine-hydrazone tautomerism of guanylhydrazones: evidence for the preference toward the azine tautomer, J. Org. Chem. 81 (2016) 7574–7583, https://doi.org/10.1021/acs.joc.6b01258.

[29] S. Diamant, I. Agranat, A. Goldblum, S. Cohen, D. Atlas, β-adrenergic activity and conformation of the antihypertensive specific α_2-agonist drug, guanabenz, Biochem. Pharmacol. 34 (1985) 491–498, https://doi.org/10.1016/0006-2952(85)90179-0.

[30] B. Holmes, R.N. Brogden, R.C. Heel, T.M. Speight, G.S. Guanabenz Avery, A review of its pharmacodynamic properties and therapeutic efficacy in hypertension, Drugs 26 (1983) 212–229, https://doi.org/10.2165/00003495-198326030-00003.

[31] C. Platella, A. Citarella, M. Manenti, G. Spinelli, R. Gaglione, A. Arciello, C. Riccardi, D. Musumeci, D. Montesarchio, C. Giannini, A. Silvani, Modular symmetric ligands for selective recognition of cancer-relevant G-Quadruplexes, J. Mol. Struct. 48 (2023) 1821–1827, https://doi.org/10.1016/j.molstruc.2023.137114.

[32] N.V. Licata, R. Cristofani, S. Salomonsson, M. Wilson, L. Kempthorne, D. Vaizoglu, V.G. D'Agostino, D. Pollini, R. Loffredo, M. Pancher, V. Adami, P. Bellosta, A. Ratti, G. Viero, A. Quattrone, A.M. Isaacs, A. Poletti, A. Provenzani, C9orf72 ALS/FTD dipeptide repeat protein levels are reduced by small molecules that inhibit PKA or enhance protein degradation, EMBO J. 41 (2022) e105026, https://doi.org/10.15252/embj.2020105026.

[33] K. Kelly Mulholland, H.-J. Sullivan, J. Garner, J. Cai, B. Chen, C. Wu, Three-dimensional structure of RNA monomeric G-quadruplex containing ALS and FTD related G_4C_2 repeat and its binding with TMPyP4 probed by homology modeling based on experimental constraints and molecular dynamics simulations, ACS Chem. Neurosci. 11 (2020) 57–75, https://doi.org/10.1021/acschemneuro.9b00572.
[34] P. Fratta, S. Mizielinska, A.J. Nicoll, M. Zloh, E.M. Fisher, G. Parkinson, A. M. Isaacs, C9orf72 hexanucleotide repeat associated with amyotrophic lateral sclerosis and frontotemporal dementia forms RNA G-quadruplexes, Sci. Rep. 2 (2012) 1016, https://doi.org/10.1038/srep01016.
[35] J.A. Bush, S.M. Meyer, R. Fuerst, Y. Tong, Y. Li, R.I. Benhamou, H. Aikawa, P.R. A. Zanon, Q.M.R. Gibaut, A.J. Angelbello, T.F. Gendron, Y.-J. Zhang, L. Petrucelli, T. Heick Jensenc, J.L. Childs-Disney, M.D. Disney, A blood–brain penetrant RNA-Targeted small molecule triggers elimination of r(G4C2)exp in c9ALS/FTD via the nuclear RNA exosome, Proc. Natl. Acad. Sci. USA 119 (2022) e2210532119, https://doi.org/10.1073/pnas.2210532119.
[36] V. Kuryavyi, A. Tuân Phan, D.J. Patel, Solution structures of all parallel-stranded monomeric and dimeric G-quadruplex scaffolds of the human *c-kit2* promoter, Nucleic Acids Res. 38 (2010) 6757–6773, https://doi.org/10.1093/nar/gkq558.
[37] P. Schultze, R.F. Macaya, J. Feigon, Three-dimensional solution structure of the thrombin-binding DNA aptamer d(GGTTGGTGTGGTTGG), J. Mol. Biol. 235 (1994) 1532–1547, https://doi.org/10.1006/jmbi.1994.1105.
[38] S. Kovachka, M. Panosetti, B. Grimaldi, S. Azoulay, A. Di Giorgio, M. Duca, Small molecule approaches to targeting RNA, Nat. Rev. Chem 8 (2024) 120–135, https://doi.org/10.1038/s41570-023-00569-9.
[39] E. Facen, G. Assoni, G. Donati, D. Paladino, A. Carreira, I. Bonomo, V. Pietra, R.-Lotti, J. Houser, L.L. Fava, P. Seneci, L. Marinelli, D. Arosio, A. Provenzani, Novel, soluble 3-heteroaryl-substituted tanshinone mimics attenuate the inflammatory response in murine macrophages, Sci. Rep. 14 (2024) 24501, https://doi.org/10.1038/s41598-024-73309-8.
[40] P. Reinhardt, M. Glatza, K. Hemmer, Y. Tsytsyura, C.S. Thiel, S. Höing, S. Moritz, J. A. Parga, L. Wagner, J.M. Bruder, G. Wu, B. Schmid, A. Röpke, J. Klingauf, J. C. Schwamborn, T. Gasser, H.R. Schöler, J. Sterneckert, Derivation and expansion using only small molecules of human neural progenitors for neurodegenerative disease modeling, PLoS One 8 (2013) e59252, https://doi.org/10.1371/journal.pone.0059252.
[41] N.R. Cashman, H.D. Durham, J.K. Blusztajn, K. Oda, T. Tabira, I.T. Shaw, S. Dahrouge, J.P. Antel, Neuroblastoma × spinal cord (NSC) hybrid cell lines resemble developing motor neurons, Dev. Dyn. 194 (1992) 209–221, https://doi.org/10.1002/aja.1001940306.
[42] Schrödinger Release 2023-1: Protein Preparation Wizard, Schrödinger, LLC, Epik, Schrödinger, LLC, New York, NY, 2023; Impact, Schrödinger, LLC, New York, NY; Prime, 2023. New York, NY.
[43] Schrödinger Release 2023-1, Maestro, Schrödinger, LLC, New York, NY, 2023.
[44] M.H.M. Olsson, C.R. Søndergaard, M. Rostkowski, J.H. Jensen, PROPKA3: consistent treatment of internal and surface residues in empirical pKa predictions, J. Chem. Theor. Comput. 7 (2011) 525–537, https://doi.org/10.1021/ct100578z.
[45] Schrödinger Release 2023-1, LigPrep, Schrödinger, LLC, New York, NY, 2023.
[46] C. Lu, C. Wu, D. Ghoreishi, W. Chen, L. Wang, W. Damm, G.A. Ross, M.K. Dahlgren, E. Russell, C.D. Von Bargen, R. Abel, R.A. Friesner, E.D. Harder, OPLS4: improving force field accuracy on challenging regimes of chemical space, J. Chem. Theor. Comput. 17 (2021) 4291–4300, https://doi.org/10.1021/acs.jctc.1c00302.
[47] R.C. Johnston, K. Yao, Z. Kaplan, M. Chelliah, K. Leswing, S. Seekins, S. Watts, D. Calkins, J. Chief Elk, S.V. Jerome, M.P. Shelley J.C. Repasky, Epik: pKa and protonation state prediction through machine learning, J. Chem. Theor. Comput. 19 (2023) 2380–2388, https://doi.org/10.1021/acs.jctc.3c00044.
[48] Schrödinger Release 2023-1: Glide, Schrödinger, LLC, New York, NY, 2023.
[49] R.A. Friesner, J.L. Banks, R.B. Murphy, T.A. Halgren, J.J. Klicic, D.T. Mainz, M. P. Repasky, E.H. Knoll, M. Shelley, J.K. Perry, D.E. Shaw, P. Francis, P.S. Shenkin, Glide: a new approach for rapid, accurate docking and scoring. 1. Method and assessment of docking accuracy, J. Med. Chem. 47 (2004) 1739–1749, https://doi.org/10.1021/jm0306430.
[50] T.A. Halgren, R.B. Murphy, R.A. Friesner, H.S. Beard, L.L. Frye, W.T. Pollard, J. L. Glide Banks, A new approach for rapid, accurate docking and scoring. 2. Enrichment factors in database screening, J. Med. Chem. 47 (2004) 1750–1759, https://doi.org/10.1021/jm030644s.